Doctoral Dissertation

Enriching Haptic Interaction with Tangible Objects by Vibration Analysis

Seungjae Oh (오 승 재)

Department of Creative IT Engineering

Pohang University of Science and Technology

2020

유형 객체와의 촉각적 상호작용을 매개하는 인식 기술 및 촉각 인지 모델

Enriching Haptic Interaction with Tangible Objects by Vibration Analysis

Enriching Haptic Interaction with Tangible Objects by Vibration Analysis

by

Seungjae Oh
Department of Creative IT Engineering
Pohang University of Science and Technology

A dissertation submitted to the faculty of the Pohang University of Science and Technology in partial fulfillment of the requirements for the degree of Doctor of Philosophy in the Creative IT Engineering

Pohang, Korea
12. 17. 2019
Approved by
Seungmoon Choi (Signature)
Academic advisor

Enriching Haptic Interaction with Tangible Objects by Vibration Analysis

Seungjae Oh

The undersigned have examined this dissertation and hereby certify that it is worthy of acceptance for a doctoral degree from POSTECH

12. 17. 2019

Committee Chair	Seungmoon Choi	(Seal)
Member	Hee-Kap Ahn	(Seal)
Member	Soohee Han	(Seal)
Member	Suseok Choi	(Seal)
Member	Jaesik Park	(Seal)

DCITE 오 승 재. Seungjae Oh
20120866
Enriching Haptic Interaction with Tangible Objects by Vibration Analysis,
유형 객체와의 촉각적 상호작용을 매개하는 인식 기술 및 촉각 인지 모델
Department of Creative IT Engineering , 2020,
116p, Advisor : Seungmoon Choi. Text in English.

ABSTRACT

Throughout our daily lives, we perform a series of tasks for the sake of achieving a specific goal. While doing so, we continuously interact with the physical environments around us as well as the artifacts within them. From this accumulated bodily experience, we have been building prevalent embodied schemas concerning environments and artifacts. Therefore, we usually perceive a shared conceptual metaphor when we encounter a specific situation or new interface. As a Human-Computer Interaction researcher, the author conducted a series of research to extend pervasive bodily actions to the realm of computing or to enhance the interaction capability of everyday environments and artifacts.

When a user interacts with everyday objects as tangible interfaces for computing, the objects need to understand the actions of the user to function as a

computing interface, meaning that the objects should be augmented with computational abilities. In the first phase of this thesis, the author explores the possibilities of vibration as a sensing channel for designing input interaction with everyday objects. First, I discuss how to augment fingers with vibration to estimate contact finger(s) when contact is made between a user and everyday surfaces. Secondly, I address how to implement and evaluate a vibration-based sensing method for the recognition of objects via their difference in the material.

For the second phase of the thesis, the author reports a psychophysical experiment that is designed to support tangible interfaces with vibrotactile feedback. Using tangible interfaces implies a series of manual interaction with tangible things. Humans require precise force control to execute fine manual tasks, which is generally facilitated to a great extent by providing adequate feedback. To design appropriate vibrotactile stimuli for such manual tasks, it is essential to quantify human vibrotactile sensitivity over a large range of contact forces. The author investigated the psychophysical detection thresholds for vibrotactile stimuli when active contact force exists. The experimental results showed stark contrasts between stimulus frequencies, depending on actively exerted pressing force.

Contents

I. Introduction **1**

1.1 Research Motivation 1

1.2 Research Goal 2

1.3 Organization 4

II. Background **5**

2.1 Preface: The Propagation of Vibration 5

2.2 Investigating The Propagation of Vibration 7

2.2.1 Preparation 7

2.2.2 Artificial Materials 7

2.2.3 Human Skin 10

2.3 Sensing Vibration for Computing Inputs 12

2.3.1 Detecting Human Action from Vibro-acoustic Signal 12

2.3.2 Recognizing Object and Material from Vibration 13

2.4 Perceiving Vibration as Sensory Stimulus 14

III. Recognizing Contact Fingers on Rigid Surfaces by Augmenting Fingers with Vibration **16**

3.1 Introduction 16

3.2 Background Experiments 18

3.2.1 Transfer Property of Vibration in the Hand 19

3.2.2 Transfer Property of Vibration on Rigid Surfaces 22
3.2.3 Transfer Property of Vibration in Electronic Devices 24
3.3 System Implementation 25
3.3.1 Hardware 25
3.3.2 Challenges and Design Considerations 26
3.3.3 System Overview 30
3.4 Evaluation 31
3.4.1 Data Collection 31
3.4.2 Preprocessing and Feature Extraction 34
3.4.3 Feature Selection and Classification 35
3.4.4 Subjective Evaluation 41
3.5 Discussion 43
3.6 Conclusions and Future Work 46

IV. Identifying Static Objects by Visualizing The Propagation Dynamics of Vibration 48

4.1 Introduction 48
4.2 System Design and Implementation 51
4.2.1 Hardware Design 51
4.2.2 Data Processing Pipeline 52
4.3 System Evaluation 56
4.3.1 Sample Sets 56
4.3.2 Recognition Performance 57
4.4 User Study 58

4.4.1 Methods 59
4.4.2 Results 60
4.5 Discussion 64
4.5.1 Summary of Results 64
4.5.2 Hardware Improvement 66
4.5.3 Vibration as A Sensory Cue 67
4.6 Applications 68
4.6.1 3D Modeling Interface for VR 68
4.6.2 Drawing Interface for AR 69
4.7 Conclusions 70

V. Investigating Effects of Contact Force and Vibration Frequency on Vibrotactile Sensitivity 71

5.1 Introduction 71
5.2 Methods 72
5.2.1 Apparatus 73
5.2.2 Participants 74
5.2.3 Stimuli 74
5.2.4 Experimental Conditions 75
5.2.5 Task and Procedure 76
5.2.6 Data Analysis 78
5.3 Results 79
5.3.1 Absolute Threshold 79
5.3.2 Pressing Force 83

5.4 Discussion 85
5.4.1 Effects of Vibration Frequency 85
5.4.2 Effects of Pressing Force 87
5.4.3 Comparisons of Absolute Thresholds 89
5.5 Conclusions 91

VI. Conclusion **92**

6.1 Contributions 92
6.2 Future Directions 93

Summary (in Korean) **95**

References **97**

List of Tables

3.1 The Comparison of Classification Performances of LOPO Cross-validation with respect to Classification Methods and Features . . 38

4.1 Prominent mappings from 18 everyday objects to standard objects (from Figure 4.8). 64

5.1 Means and Standard Deviations of Force Control Error (***CtrlErr***), and the Means of Accuracy and Precision 83

5.2 Comparison of Detection Thresholds in Peak Displacement Amplitude of Sinusoidal Vibrations Transmitted to the Fingertip for Two Frequencies and Two Pressing Forces (units are in dB re 1 μm; † denotes interpolated values; underlinefor static force cases and **bold** for active force cases). 90

List of Figures

3.1 Overview of interaction with our system. A user wearing our vibration rings makes contact on a rigid surface with microphone attached (left) and on an electronic device with its internal microphone (right). 18

3.2 An experimental setting for the transmissibility of the hand (left). 11 surface transducer positions over the hand (middle) and three contact sites (right). 20

3.3 The transfer properties over the hand. *finger pad* (blue), *fingertip* (red), and *nail* (yellow). 21

3.4 An experimental setting for the transmissibility of rigid surfaces . . 23

3.5 The transmissibility measurements of rigid every surfaces at three different distances (right). *acrylic* (blue), *glass panel* (red), *zinc-coated MDF* (yellow), and *concrete wall* (green). 23

3.6 The transfer properties for the tablet (left) and the wireless earbuds (right). 25

3.7 Our wearable ring-type hardware and stereo amplifier module. A 3D model of the hardware (left), its 3D printed model with a transducer (middle), and the amplifier module (right). 26

3.8 Sound samples from our recoding platform. 30

3.9 A recording sample from our system. 32
3.10 The spectral information of six contact finger conditions using FFT. 34
3.11 The three distribution of the collected data. From left to right, the raw FFT values of the three encoded frequencies, the normalized FFT values of the frequencies, and the first three principal components. Each distribution has six following groups: Thumb (T; red), Index (I, green), Middle (M, blue), Thumb+Index (T+I, olive), Thumb+Middle (T+M, purple), and Index+Middle (I+M, turquoises). 36
3.12 The performance measurements of SVM classifiers depending on the number of principal component features. The left axis presents for the mean accuracy (blue bars) and its standard deviations (blue error bars) of LOPO cross-validation models. The right axis is for the mean computation time (orange bars) and its standard deviation (orange error bars). 39
3.13 The confusion matrix of the classifier of each classification method. For each confusion matrix, the recall and precision of each class are presented. 41
3.14 The mean scores of all subjective ratings. Error bars represent standard errors. 42

4.1 VibEye: system overview and operation principle (left). Data processing pipeline (right-top). A classification model is built from 16 standard objects and then applied to categorize 25 everyday objects (right-bottom). 49
4.2 Hardware design of VibEye. 52
4.3 Computational procedure for signal processing and object recognition. 53
4.4 Spectrograms of 16 standard objects. Objects are marked with material properties (R: rigid, E: elastic, V: viscous, P: plastic, and S: stacked). The cutoff level δ was -38 dB. The cubic objects that we molded from liquid materials are specified with the material manufacturers and models. 55
4.5 Twenty-five everyday objects. 58
4.6 Confusion matrix for recognizing standard objects. 60
4.7 Precision and recall for standard objects. 61
4.8 Confusion matrix for categorizing 25 everyday objects to 16 standard objects. 63
4.9 Another four sets of everyday objects and their PCA results (20 repetitions each): (A) Liquid body products in soft tubes, (B) candies in hard containers, (C) stacked papers, and (D) a spray bottle (empty or full). 66
4.10 Applications of VibEye: (left) VR 3D modeling and (right) AR drawing tool. 68

5.1 Experimental setup. 74
5.2 Absolute thresholds in terms of peak displacement in dB measured in all experimental conditions. Error bars show standard errors. . . 80
5.3 Absolute thresholds in terms of peak displacement measured for each ***Freq*** condition. Error bars show standard errors. For each frequency, data points marked with different letters were different with statistical significance. 81
5.4 Mean force control errors with standard errors (error bars) for each frequency and the existence/absence of vibrotactile stimulus. . . . 84

I. Introduction

1.1 Research Motivation

Direct manipulation has been a leading paradigm of user interface research for past decades. The concept facilitates advances in computing technologies with its directness in interaction [1, 2, 3]. The metaphor of direct manipulation is closely related to the level of directness between physical action and its representation, and the direct manipulation metaphor can be characterized into a continuum suggested by [4]. Manipulating tangible objects for computing (strong direct manipulation [4, Box 7.1]) provides meaningful direct manipulation metaphor [4] because the tangible interaction utilizes dexterous and innate haptic interaction skills and rich physical affordances of the objects [5, 6]. In other words, the tangible computing interfaces are inseparable from haptic interaction, and various haptic feedback, e.g., vibration, kinesthetic, and thermal, has been frequently used to mediate interaction with tangible computing interfaces. This dissertation focuses on the usage of tangible interfaces with vibrotactile feedback. From a series of studies, the author explores how the fundamental understandings from the propagation dynamics of vibration can enhance haptic interaction with tangible objects and vibrotractile feedback.

1.2 Research Goal

The concept of gulf-of-execution and gulf-of-evaluation represents the gap between a person's goals and representations from the system [2, Figure 3]. When a person interacts with computing systems, there should be appropriate sensory representations to be understood by the person. On the other side, when a person performs an action to the system, the action is not meaningless only when that action can be perceived by the system. This dissertation describes a series of works that bridges the gap when interacting with tangible props for computing purpose.

The gulf of execution will be successfully bridged by designing appropriate inputs reflecting the context of computing. For tangible interaction, contact is always there when a user interacts with a physical medium for computing, and this also implies that the user grasped some tangible thing. In this thesis, the author focused on bridging the gulf of execution in tangible interaction by answering the following two questions: 1) identify contact between a user and an object and 2) recognize the object grasped by the user.

The contact provides valuable information on the contact state in two categories: one about the contact itself (contact point, force, and duration) and the other about the hand making the contact (contact fingers and hand posture). Sensing such fundamental properties of contact leads to more convenient and expressive tangible interaction. Therefore, the advance in sensing techniques that articulate the major properties of contact can significantly improve usability and user experience in the interaction mediated by tangible objects. In this regard,

the author introduces a novel approach to identify contact fingers by augmenting the hand with vibro-acoustic signals.

Recognizing objects of interest affords opportunities to a computing system to assume the user's context [7, 8]. Such context-awareness has the potential to enrich interaction by providing relevant functionalities [9, 10]. Further, the material that an object is made of reinforces the context [11, 12]. The recognized information enables the object to function as a part of the computing environment. Therefore, we focus on how to recognize hand-held objects based on their differences in material in order to support tangible interaction in various computing contexts and environments.

To bridge the gulf of evaluation by presenting vibrotactile feedback to a user with tangible interfaces, the first thing to do is to identify the sensory channel. What characterizes the tangible interaction from the others is the high degree of freedom in manual tasks. In such tasks, vibrotactile feedback is perceived in the presence of external pressure to contact sites, e.g., fingertip. Therefore, understanding the effects of contact force on the perception of vibrotactile stimuli is a prerequisite for designing dexterous manual interaction in tangible computing with vibrotactile feedback. To clarify the sensory channel of vibrotactile stimuli, the author investigated the vibrotactile sensitivity of the fingertip about the two major factors: 1) a wide range of contact forces encountered during ordinary manual tasks and 2) two vibration frequencies innervating two different tactile sensory channels.

1.3 Organization

The rest of this thesis is structured as follows. In Chapter II, the background on the nature of vibration and its propagation is described, which includes the propagation of vibration on the two most relevant mediums, human skin and artificial materials. Chapter III explains how to identify contact finger(s) on rigid surfaces when the fingertip is augmented by vibration. Chapter IV introduces the vibration-based sensing framework for object recognition. In Chapter V, the author states the detailed analysis on vibrotactile sensitivity under active contact force.

II. Background

2.1 Preface: The Propagation of Vibration

Vibration is a mechanical wave that oscillates through a medium while transferring energy. The propagation of vibration is largely affected by the mechanical characteristics of a medium. Our interdisciplinary study is all starting from the observation of vibration and the analysis of its propagation.

The first medium to discuss is human skin. In haptic research, the medium of vibration is human skin, and the main focus is to see how the propagation of vibration activates the sensory receptors of vibratory stimuli. Verifying external factors having an influence on the vibration propagation is of importance, such as contact pressures, contact postures, contact sites, and configurations of a contactor. Such quantitative observations provide evidence for the understanding of vibrotactile perception. For input technologies in Human-Computer Interaction, the same information about the vibration propagation within human skin is utilized to devise sensing methods in many ways, e.g, design on-body interaction, estimate hand gestures or poses, and identify users.

Secondly, the other medium for vibration analysis is artificial materials and objects. When exposed to a forced vibration, a medium of mechanical vibration is modeled by the combination of the three impedance terms, a mass, a spring, and a damper, where each term is a function of vibration frequency. This model–

mechanical impedance–predicts how vibration is attenuated while transmitting a medium. The transmissibility of vibration across a medium is also affected by other external factors, such as the shape of an object and its material composition, that contribute to the boundary conditions of differential equations. With the emphasis on the difference in the vibration propagation dynamics, several attributes of vibration, e.g, resonance frequency and transfer function, have been used to discriminate materials or objects in Human-Computer Interaction studies. In Haptics, the information is used to improve the quality of vibrotactile stimuli. Sometimes, the resonance profile of an object of interest is examined to select effective frequency ranges to be delivered to human skin. Conversely, a material with a high absorption rate in the frequency of interest is sometimes attached to localize the tactile stimuli within a specific region. In the following sections, the author deep dives into the listed topics to illustrate previous literature and to provide an insight for future studies.

The research goals of this thesis are based on the analysis of vibration propagation, and each deals with a different medium for vibration to travel: rigid surfaces and the hand (Chapter III), objects made of different materials (Chapter IV), and human skin (Chapter V). Section 2.2 summarizes the literature about the propagation of vibration over human skin and artificial materials, and the author describes several considerations for designing vibrotactile feedback or implementing vibration-based sensing techniques. Section 2.3 describes the frameworks of sensing techniques utilizing vibration and the review of the previous literature. In Section 2.4, the description of the vibration propagation across

human skin helps understand the response of sensory receptors responsible for vibrotactile perception.

2.2 Investigating The Propagation of Vibration

2.2.1 Preparation

The first step is to select and characterize an actuator. The actuator is the hardware that produces physical vibration, which should be carefully selected depending on the constraints and goals of the final vibrotactile display [13]. For tactile displays, it is of critical importance that the selected actuator should be calibrated to ensure the reproducibility of results. The calibration of the actuator is to find the relationship between the input, e.g., voltage or current, that is assigned to the actuator and the output, e.g., acceleration or displacement, that the actuator presents from the input. For sensing purposes, what is most important is to check whether the actuator-sensor pair can display and capture signals with the intended range and accuracy. When it comes to vibration for feedback, the perceived intensities of vibrotactile stimuli are sometimes matched, instead of the physical amplitude of vibration.

2.2.2 Artificial Materials

The vibrational response of a structure is simply modeled by using the three terms, a mass (m), a spring (k), and a damper (c), and solving differential equations tell how a force vibration affects the motion of the structure. There are some hyperparameters, e.g., the critical damping (c_c), the damping ratio (ζ), and the

natural frequency (w_n), that help understand the response of the structure. The critical damping ($c_c = 2\sqrt{km}$) tells about the value that a system does not vibrate if its damping coefficient is larger than or equal to the critical damping. The damping ratio ($\zeta = \frac{c}{c_c}$) is the ratio between the current damping and critical damping of the current system, which allows us to simply catch how the system will behave under forced vibration. The natural frequency ($w_n = 2\pi f_n = \sqrt{\frac{k}{m}}$) describes the frequency where the amplitude of vibration is maximized, and this phenomenon is called resonance.

For rendering vibrotactile stimuli, we mostly concern about underdamped cases ($c < c_c$), and the solution of the underdamped system can be found in Equation 2.1.

$$x(t) = Xe^{-\zeta w_n t} cos(2\pi\sqrt{1-\zeta^2} f_n t - \phi) \tag{2.1}$$

In this equation, there exist two terms that describe the response of the system. The multiplication of the damping ratio and natural frequency in the exponential term denotes how fast the forced vibration is decaying, and the frequency of the cosine term explains that the higher the damping ratio is, the slower the oscillation of the vibration is.

When it comes to real-world problems, estimating the propagation of vibration is not as simple as the computation in the described theoretical model because of several reasons like complicated structures, nonlinear properties, complex boundary conditions. Despite such complex nature, vibration analysis has been applied in many areas like monitoring the structural health, detecting malfunctions, designing facilities, alarming earthquakes, and selecting attenuation

material. Instead of directly solving equations, many practitioners measure the transmissibility of vibration while varying frequency [14, 15, 16], which is to figure out the impedance terms that are functions of frequency.

In Haptics research, the vibration attenuation property of materials is utilized to localize tactile stimuli around contact. The commonly used isolation materials are silicone [17], polyurethane [18, 19], sponge [20], sorbothane [21], and steel spring [21], and these are the materials having high damping constant. Park et al. report the attenuation of vibration on elastic silicones (EcoFlex 0010 and 0030; Smooth-on) over the wide range of vibration frequencies and amplitudes, and the usage of the 3-mm silicone layer effectively blocked vibration transmission, especially frequencies over 200 Hz (> 90 %).

Conversely, the vibration transmissibility of materials needs to be improved to detect vibration signals for sensing purposes [22, 23, 24, 25, 26, 27]. For vibration sensing, it requires to select the material transmitting the frequency range that includes significant spectral information. Therefore, it is important to matching stiffness and weight for the right natural frequency. As another factor for vibration propagation, Fabiani [22] reports that the isotropic material, e.g., glass, is better to transmit vibration signals than the anisotropic materials, e.g., wood and MDF, because of unexpected phase differences resulting from the irregular microstructure of anisotropic materials. The vibration transmissibilities of materials have provided insights into the sensing principles of our suggested sensing techniques.

2.2.3 Human Skin

Once an actuator is activated, the vibration emanating from the actuator is transmitted directly to the skin that is making contact with the vibration source. Therefore, the profound understanding of the propagation of vibration over human skin is the core factor in designing good vibrotactile stimuli. In summary, the forced vibration on human skin presents high transmissibility when: 1) the distance from the vibration source is close (< 30 mm); 2) the frequency is low (< 160 Hz); 3) both the contact force (> 4 N) and the frequency is high (> 200 Hz).

The transmissibility of vibration is largely affected by body site [28] and frequency [29, 14, 30]. First, the amplitude of vibration attenuates to approximately 30 % at 8 mm and to 25 % at 24 mm away from the vibration source on the palm [28] where the frequency of the observed vibration is around 70 Hz (3 V; pancake motor). When they tested the same actuator at different body sites, such attenuation rates were more rapid at the forearm and thigh where the skin stiffness is lower than the palm. Recently, Dandu et al. [29] precisely measure the propagation of vibration from the index fingertip with the shaker and laser doppler vibrometer, varing frequencies from 40 to 640 Hz in steps of 40 Hz, and the distances with the half of the energy (D(f)) in each frequency are recorded. The lower frequencies (< 160 Hz) travel further (D(f) > 40 mm) from the fingertip to the hand, and the highest frequency, 640 Hz, presented the half of the total energy at the distance less than 30 mm [29].

The mechanical properties of the hand are affected by contact conditions

like hand posture [30], contact area [14], and contact force [30, 31], which influences the transmissibility of vibration across the skin. In general, the mechanical impedance of the hand [14, Figure 5] increases as vibration frequency increases toward roughly 100 Hz, and then, the impedance starts to increase again around 300 Hz. The increase in the mechanical impedance decreases the transmissibility of vibration. This result is consistent with the transmissibility measurement by [30] where the transmissibility significantly decreases after 2-300 Hz. Schaefer et al. measure the transmissibility of the sinusoidal sweep (20 to 500 Hz) from the fingertip to the three different phalanges on the index finger (in the middle of the distal, middle, and proximal phalanx) with three different postures [30]. The transmissibility degrades as the signal is measured at the phalanx close to the base of the finger, and the three postures present slightly different trends in the vibration transmissibility. When the sweep signal is measured close to the vibration source, the effect of the postures is not significant regardless of frequency; however, a straight finger with normal contact transmits vibration toward the proximal phalanx slightly better than the other postures. Although the higher contact force increases the mechanical impedance of the distal phalanx of the finger except the frequency between 60 to 80 Hz [31], the vibration transmissibility is not affected significantly or even improved in the frequency beyond 250 Hz when force increased from 4 N to 15 N [30].

2.3 Sensing Vibration for Computing Inputs

2.3.1 Detecting Human Action from Vibro-acoustic Signal

The transmission of vibration within the hand and arm are presented in Section 2.2.3. In this section, the author highlights studies that designed input techniques exploiting the transmission of vibration within the human arm. There have been mainly two approaches for input sensing methods using vibration: 1) Detect the inevitable and typical vibration patterns generated by human action and 2) Observe the distortion of a structured vibration from human action.

The former is designed to capture vibration and sound transmitted from contact and gesture. There have been several attempts to recognize contact position with piezo-electric sensor(s) attached to the arm [32] or wrist [33], trying to reduce the number of sensors while not compensating accuracy. These estimation methods for on-body contact position are extended to surfaces [34] or implemented with a commercial wearable device [35]. To reflect more situated interaction, vibrations made from gestures are detected by wearable watch [10].

The other approach uses both sensor and actuator pairs to detect users' actions. It is possible to estimate contact force [25, 36] and contact position [26, 37] with the sensor and actuator pairs attached to flat rigid surfaces or rigid objects. In addition, sending a vibration to the hand enables the estimation of grip force [38], finger joint angle [39], and hand postures [40, 41]. Also, it is possible to design an authentication method using hand resonance profiles [42]. In most cases, frequency sweep signals generated by surface transducers are measured by contact microphones, e.g., piezoelectric sensor and piezo-ceramic accelerometer.

2.3.2 Recognizing Object and Material from Vibration

A mechanical vibration that propagates through a medium leaves a unique signature. Research on vibration-based sensing for object recognition has followed two strategies: active object sensing and passive object sensing. The former is to detect the patterns of vibrations emanating from an object that encompasses its own oscillation source, e.g., motor-powered vibrating objects. ViBand [10] measures a vibration transmitted through the human body to recognize the object that has generated the vibration. Vibrosight [43] remotely detects unique vibration patterns of objects in operation with laser vibrometry. While useful, these methods are not applicable to still objects.

The other approach is to apply a structured vibration (e.g., sinusoidal frequency sweep) to a static object and measure the response, and then compare the input and output (I/O) signals for object recognition. This approach works with any objects although it requires an external vibration source. Kunze et al. [44] and Cho et al. [7] find the location of a mobile phone by measuring acceleration (and also sound [44]) using internal sensors after imposing a vibration. These studies envision the possibility of material recognition from vibration signatures. VibeBin [23] takes advantage of resonance when the object is exposed to vibration. This system learns the discrete fill-levels of a waste bin and then classifies them using clustering.

2.4 Perceiving Vibration as Sensory Stimulus

The vibration propagating across the skin is detected by sensory receptors in the skin.There are mainly four cutaneous mechanoreceptors responsible for tactile sensation, and two are located in the outer layer of the skin (epidermis) and the other two reside deeper underneath the skin (dermis) [45]. Each receptor has a different receptive field size and biomechanical structure resulting in handling different types of tactile stimuli. In terms of vibrotactile feedback, we mainly consider two fast-adapting mechanoreceptors, the Pacinian and Meissner corpuscles, each of which is in charge of perceiving rapid and transient signals but different frequency ranges. According to the literature [46, 47], Pacinian corpuscles located in the deeper layer with a larger receptive field and sparse density are responsible for higher-frequency vibrations (40-400 Hz), and Meissner corpuscles found just beneath the epidermis detect lower-frequency vibrations (5-50 Hz). The distribution of both receptors are fairly low over the hairy skin, e.g., forearm, thigh, and torso, compared to the glabrous skin, e.g., the hand and fingertip [48].

There are noticing results on the vibration propagation in conjunction with the characteristics of the mechanoreceptors. Vibration travels further through the hand as its frequency decreased in general [29]. As such, this propagation trend of vibration should be considered with the response of fast-adapting mechanoreceptors when designing a vibrotactile display with multiple distant actuators. As denoted in the previous section, the existence of contact force improves the transmissibility of vibration deeper in the skin, especially the frequencies higher than 200 Hz [30], and one possible explanation is the compressed skin tissues bet-

ter coupling vibrations transmitted to bones and tendons [49, 50]. This implies that actively pressing a vibration source increases the possibility of activating the Pacinian corpuscle lying deep in the dermis, but not the Meissner corpuscle. In summary, it is of importance to understand the sensory capability in human vibrotactile perception for truly meaningful haptic experience, but it is essential not to miss how vibration innervating the sensory receptors is delivered through the skin.

III. Recognizing Contact Fingers on Rigid Surfaces by Augmenting Fingers with Vibration

3.1 Introduction

The limited input vocabulary is one of the key obstacles that hinder the usage of tangible interfaces. To increase the input bandwidth of tangible interaction, We explore the possibility of an input sensing method that identifies contact fingers on rigid surfaces using vibration. There has been a number of previous attempts to discern finger(s) of a user, and they can be mostly summarized into two approaches, implicit and explicit finger identification.

The first approach infers contact fingers from the highly correlated actions and states, e.g., postures of the hand [51, 52], contact states of the finger [53, 54], the arrangement of hands [55], fingerprints [56], and muscle tension [57, 58]. Because of inevitable ambiguities, this approach mostly presents low classification accuracy (mostly around 80-90 %) and limited sensing capabilities (2-3 single finger contact). To overcome these limitation, researchers encode fingers with explicit marker or hardware, including visual markers [59, 60], vibration motor [61], motion sensors [62, 63], and distance sensors [64, 65]. These explicit methods present decent accuracies, but they mostly do not support multiple simultaneous contact fingers or require special-purpose hardware.

In this chapter, we suggest an active sensing technique that is capable of identifying multiple simultaneous contact fingers. For that purpose, we implement our hardware with existing a form factor, a ring to actuate vibration, and an off the shelf sensor, a microphone inside commercial wireless earbuds. A user can interact with rigid surfaces just by attaching a sound recording platform (Figure 3.1, left), which is also possible to use rigid objects having a microphone inside (Figure 3.1, right). We envision that touch interaction can be nearly anywhere as wanted.

Specifically, we augment each finger with a vibrating ring to encode single vibration frequency, and a recording platform that is slightly modified from commercial wireless earbuds captures the vibration activated from the rings. The activated vibration is transmitted from the finger to the microphone inside the earbuds, traveling across the finger and a rigid surface. Through a series of background experiments enlightening this vibration propagation, we adopted a few vibration frequencies that are eligible for this purpose. We also tested electronic devices that are already equipped with its internal microphone.

For the vibratory augmentation of the finger, we implemented a flexible ring-type device equipped with a surface transducer (Figure 3.7). We also designed our recording platform to be attachable and detachable, which makes it more flexible to capture the signal propagating from the ring-type wearable. To avoid unpleasantness in using this interface, the wearable ring presents vibration only once, as weak and short as possible, whenever contact between a user's finger and a surface is detected. For detecting contact to initiate interaction, we imple-

mented an impulsive sound detection algorithm detecting tapping sound made between the user and a surface.

Using the system, we collected 1463 samples from 11 participants to train and test classification models that discriminate three contact fingers and three multi-touch combinations among them. The best classifier trained by Support Vector Machine presented 96.03 % of classification accuracy. In summary, we suggest a vibration-based sensing technique that identifies contact fingers by emitting encoded vibration from a finger and detecting the encoded signal at the surface having contact with the finger. This vibratory augmentation of fingers enables computing environments to retrieve rich contact information.

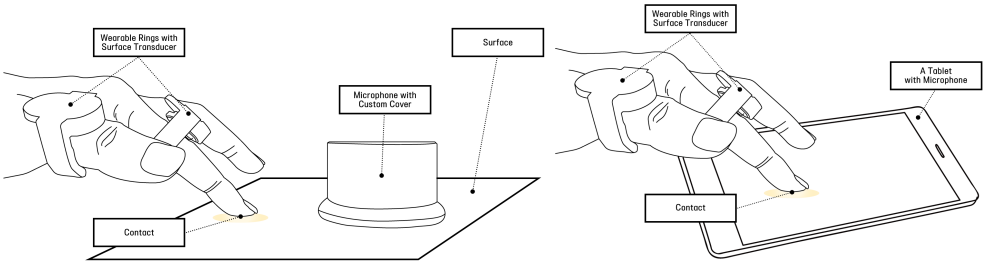

Figure 3.1: Overview of interaction with our system. A user wearing our vibration rings makes contact on a rigid surface with microphone attached (left) and on an electronic device with its internal microphone (right).

3.2 Background Experiments

In the suggested interaction, a surface transducer on the hand injects a vibration, and the vibration travels to the fingertip. The surface (or object) having contact with the fingertip is exposed to the vibro-acoustic signal. Finally, the

signal travels to the microphone that is attached to the surface or is mounted in the object. As described, the transmission of vibration can be divided into two phases: 1) From the hand to the fingertip and 2) From the contact to a microphone. Although there have been plenty of previous attempts to use vibration for detecting human actions [25, 36, 26, 37, 39, 38] and hand gestures [10, 40, 41], none of them inspected the sensing possibility of vibration traveling through two sequential mediums, e.g., the hand and surface. Therefore, we checked the feasibility of the sensing channel before we move on to the next step. In this section, we report the transmissibility of vibration in each phase to examine the possibility of signal detection and investigate parameters that influence the quality of signals.

3.2.1 Transfer Property of Vibration in the Hand

We first investigated the transmission of vibration from the hand to the fingertips varying actuation position and contact site as shown in (Figure 3.2). A surface transducer (PUI Audio; ASX02108R) displayed an exponential chirp from 300 to 3000 Hz for 1 s, and the vibration signal was amplified by a 3.1 W mono audio amplifier (Texas Instruments; TPA6211A1EVM). A contact microphone (Knowles; BU-27173) recorded the vibration transmitted to the fingertip. We captured signals with a contact microphone to ensure that the signals are from structure-borne propagation, not air-borne propagation [36, 66]. A data acquisition unit (National Instruments; USB-6251) controlled input and output data with the sampling rate of 44.1 kHz.

The vibration exciter was attached to one of the 11 positions (Figure 3.2,

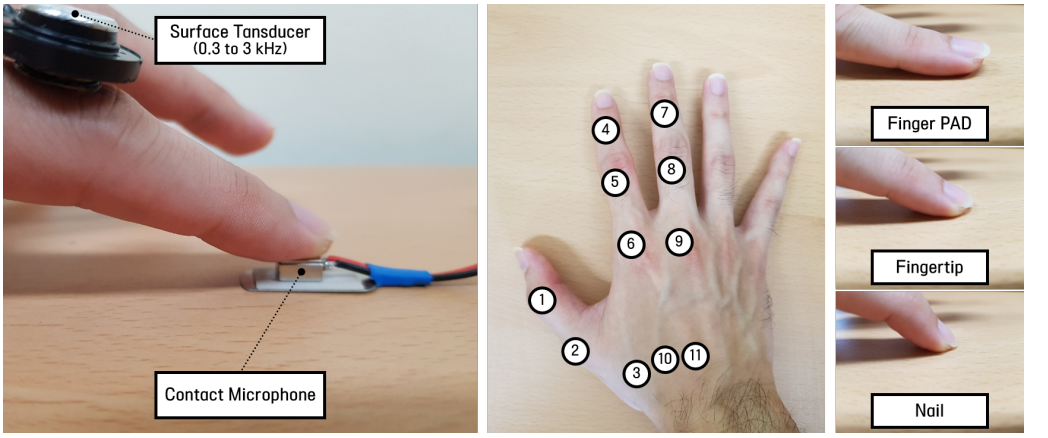

Figure 3.2: An experimental setting for the transmissibility of the hand (left). 11 surface transducer positions over the hand (middle) and three contact sites (right).

middle), the beginning of phalanges (middle and proximal for *Middle and Index*; proximal for *Thumb*) in each finger & the beginning and ending of metacarpals in each finger. For each actuation position, we recorded the vibration at the fingertip of one of three fingers, *Thumb*, *Middle*, and *Index Finger*, where the the transducer was located. To investigate whether contact sites affect signal quality, we captured the transmissibility with three common contact sites, *fingertip*, *nail*, and *finger pad* (Figure 3.2, right). In total, we collected 33 recordings each (11 ***position*** $\times$ 3 ***contact site***) from five participants. We computed frequency responses from the estimation of impulse response with the exponential sine sweep method [67].

The resulting frequency responses are presented in Figure 3.3 to represent the transmissibility. At all positions, *finger pad* resulted in the lowest transmis-

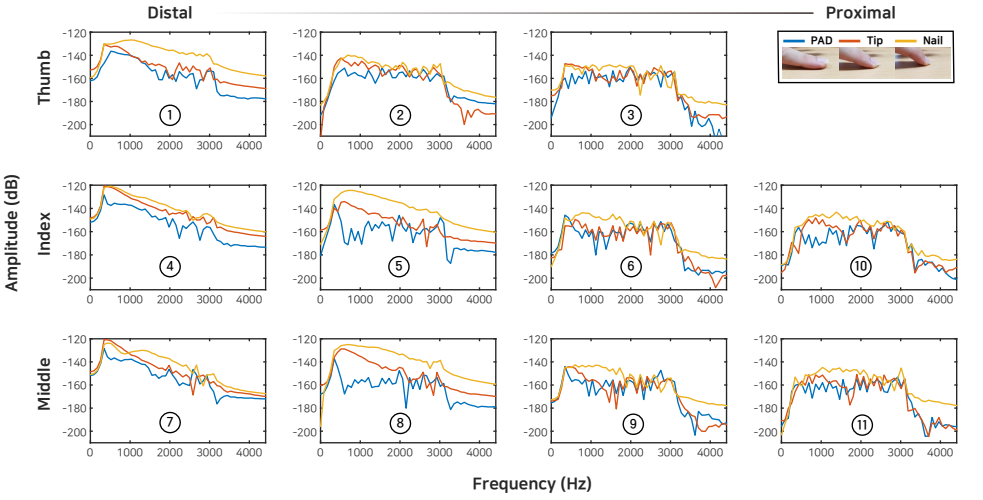

Figure 3.3: The transfer properties over the hand. *finger pad* (blue), *fingertip* (red), and *nail* (yellow).

sibility when compared to *fingertip* and *nail*, and *nail* could transfer frequencies beyond 1 kHz better than *fingertip*. When the positions of the transducer goes far from the fingertip, the transmissibility degrades to -150 dB even at the highest values (position 10 and 11) and sometime only the nail-contacted posture could deliver vibration to the fingertip (position 3, 6, and 9). We observed that the transmissibility of *thumb* were lower than the other two fingers in general. Thus, we chose position 1, 5 and 8 where signal intensities were balanced between the three fingers. Consequently, a ring is the best form factor to place transducers on those three positions.

3.2.2 Transfer Property of Vibration on Rigid Surfaces

As the second phase of the sensing channel, we first examined the propagation of vibro-acoustic signals over several rigid surfaces made of different materials. We used a microphone and a Bluetooth unit in wireless earbuds (QCY; T1S) to record vibro-acoustic signals, and a double-sided tape is attached to fix their position. A cylinder-shaped custom cover enclosed the wireless microphone unit to reduce external noise and the human voice. This wireless recording platform can be freely attached and detached by using a reusable adhesive gel tape. For data acquisition, we used the internal sound card (Realtek; ALC887) of the desktop, and the other experimental settings are the same as the previous section 3.2.1.

The recording platform was attached to the center of a surface, and a surface transducer was attached to the surface with the distances varying from 4, 7, and 10 cm from the platform (see Figure 3.4). For surface materials, we chose various anisotropic and isotropic materials: *acrylic* (density: 1.18 g/cm^3; Isotropic), *glass panel* (2.70 g/cm^3; Isotropic), *zinc-coated MDF* (7.14 g/cm^3 (zinc); Anisotropic+Isotropic), and *concrete wall* (2.30 g/cm^3, typically; Anisotropic). The same exponential chirp (300 to 3000 Hz, 1 s) was displayed to acquire frequency responses.

The frequency responses are presented in Figure 3.5. The transmissibility of *zinc-coated MDF* (yellow) little degraded as the distance increases in general, but we could not find no regular patterns. The transfer functions of the other three materials, *acrylic* (blue), *glass panel* (red), and *concrete wall* (green), were not

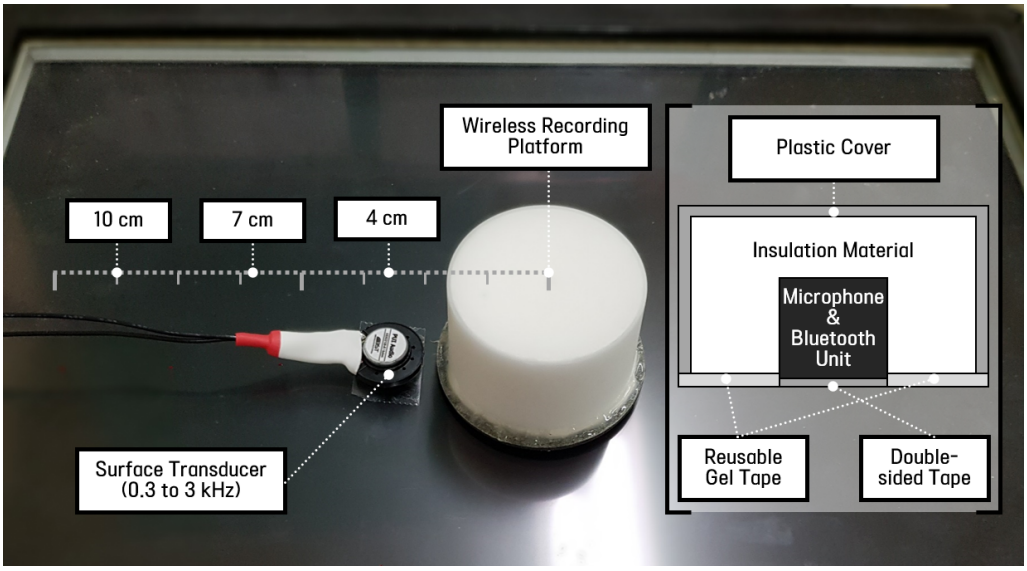

Figure 3.4: An experimental setting for the transmissibility of rigid surfaces

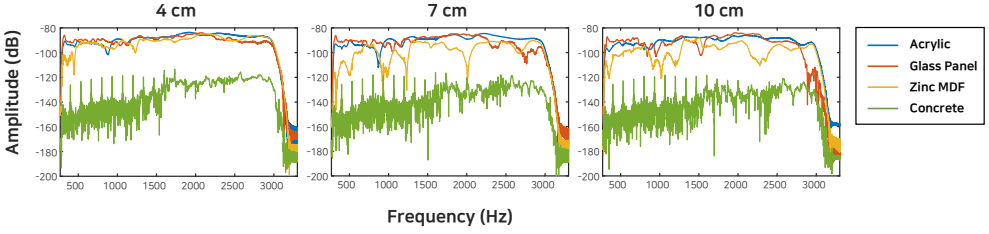

Figure 3.5: The transmissibility measurements of rigid every surfaces at three different distances (right). *acrylic* (blue), *glass panel* (red), *zinc-coated MDF* (yellow), and *concrete wall* (green).

much affected by the distance, and the two isotropic material surfaces, *acrylic* and *glass panel*, presented good vibration transmissibility regardless of the distance and frequency. *concrete wall* did not transmit signals at all since the material is

well-known for its sound blocking property. All in all, it would be easier to select frequencies to be encoded if isotropic materials are available.

3.2.3 Transfer Property of Vibration in Electronic Devices

For the second phase of the sensing channel, we also tested two electronic devices having a microphone inside in themselves: wireless earbuds (QCY; T1S) and a tablet (Google; Nexus 7). The purpose of this test is to verify whether it is possible to detect the vibration transmitted from the finger at rigid objects having a microphone inside. If successful, it means that it is available to communicate with objects equipped with a microphone, such as IoT devices, remote controllers, and Bluetooth speakers, via vibratory augmentation of fingers. We collected signals at equally spaced six grid positions over the tablet; for the wireless earbuds, a single spot near its button interface. We covered microphone holes to reduce external noises and to prevent detecting air-borne propagation. Other experimental settings and procedures are more or less the same as the previous section (Section 3.2.2).

The frequency responses of the electronic devices are presented in Figure 3.6. First of all, the vibro-acoustic signal within the electronic devices was captured as fairly good quality when it is close to a microphone (Figure 3.6, Top Left (dark blue) and Top Right (dark green) & At Button (pink)). For the tablet, the propagation of vibro-acoustic signals generally degraded when it gets far from the microphone located at the top left side, and it was not possible to observe regular patterns in regard to frequency. We assume that such unexpected trends in the vibration transmissibility of electric devices are due to their complex configuration

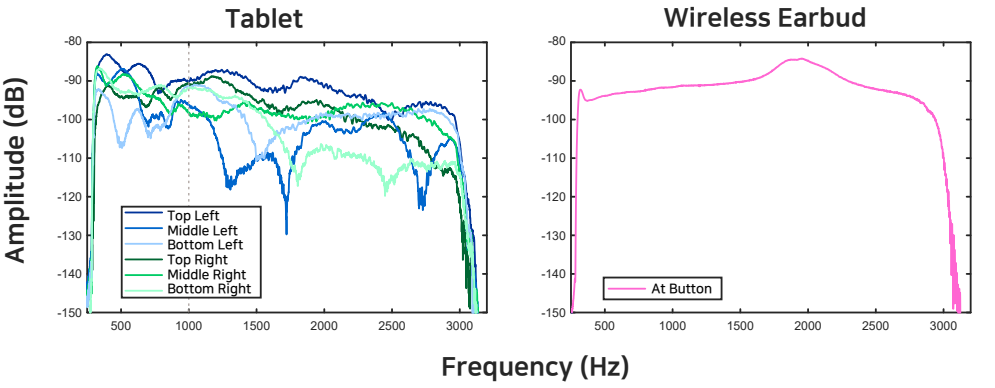

Figure 3.6: The transfer properties for the tablet (left) and the wireless earbuds (right).

inside. Although not the very best, the amplitudes of the detected signal were acceptable without significant drop down for the frequency lower than 1 kHz.

3.3 System Implementation

3.3.1 Hardware

For everyday surfaces to capture the signal, we implemented the recording platform described in Section 3.2.2. The platform can make a wireless connection with a computer to transfer microphone recordings, and this is freely attached and detached to flat surfaces. A cover of this platform enclosed hardware and blocked external sound by approximately -3.69 dB of signal power compared to when it is open. For electronic devices, we used the internal microphone of the devices with its microphone hole covered, and microphone recordings were transmitted to a computer by using Bluetooth connections.

Figure 3.7: Our wearable ring-type hardware and stereo amplifier module. A 3D model of the hardware (left), its 3D printed model with a transducer (middle), and the amplifier module (right).

We designed ring-type wearable hardware both comfortable to use and flexible to individual difference (Figure 3.7). The inner diameters of the hardware are 14.2, 15.8, 18 mm to handle different sizes of the three fingers and individuals. The material for the hardware needs to be elastic and bendable (Stratasys; Tango Plus [68]) to ensure its comfort of use. All of the listed hardware was controlled by 44.1 kHz of the sampling rate.

3.3.2 Challenges and Design Considerations

From a series of the background experiments, we reviewed the possibility of detecting vibrations that travel through the hand and a succeeding rigid surface. With these observations and previous findings, we explored how to how to design the interface that detects the vibration reliable but unobtrusive as possible. For this purpose, we need to carefully select vibration parameters like amplitude, frequency, and duration. When it comes to perceptual aspects, we want the

vibration and sound caused by it to be less perceptible, which means that the amplitude of the vibration should be as low as possible. There exists a contradiction because this will lower the quality of detected signals at the sensor end. Moreover, vibration frequency significantly affects both vibration transmissibility and human perceptual sensitivity; therefore, we tried our best to set up the rules to select optimal frequencies that satisfy both of them.

Our approach is basically encoding a single frequency to each finger and decoding the frequencies to identify contact finger(s). It does not make problems when a single finger makes contact since recognizing a contact finger is simply done by detecting the single encoded frequency. However, detecting multiple contact fingers means that we need to detect multiple frequencies from different fingers, and vibrations from both fingers should transmit well without interfering with each other. In the following sections, we will explain how we design the system based on the listed challenges.

Human Perception of Vibration and Sound

The perceptual sensitivity of two sensory channels, auditory and cutaneous, was reflected in our frequency selection. First, we considered human vibrotactile sensitivity on frequency. If we take a look at equal sensation contours for vibration [69, Figure 7][70, Figure 2], the vibrotactile sensitivity is the highest at frequencies around 250 Hz. The tactile sensitivity becomes less sensitive as frequency increases, and the sensory receptors do not react to the vibration frequency beyond 1 kHz [70]. Therefore, it is reasonable to use frequencies beyond 250 Hz and as high as possible to design a less perceptible but reliable vibra-

tory communication channel. Conversely, the auditory sensitivity increases as frequency increases to 1 kHz, and the sensitivity reaches its plateau until approximately 1.7 kHz, according to equal-loudness contours in [71, 70]. As such, it is inevitable for us to balance between these two criteria. When we chose vibration frequencies to be encoded, we considered both these perceptual aspects and signal qualities.

Vibration and Transmissibility

From the background experiments (Section 3.2.1), we found several notable factors, e.g., contact site, finger, vibration frequency, and actuation position, that affects the propagation of vibration. When contact is made by touching a surface with finger pads, only lower frequency vibrations (300-400 Hz) reached the fingertip, and we decided not to consider the contact site because of high vibrotactile sensitivity in such frequencies and discomforts from making contact with such posture. Our next concern is to match transmissibilities between fingers by choosing appropriate vibration frequency. The thumb presented distinguished transmissibility results compared to the other two fingers. The vibration propagating from the thumb did not transmit well due to the finger's larger mass, and the finger presented local maximums before 500 Hz at all contact sites (see Figure 3.3 for position 1). For successful signal transmission, the thumb needs to be augmented with the lowest frequency among the three fingers. Not a significant difference, but we found the middle finger better transmitted higher frequencies (>500 Hz) than the index finger (see Figure 3.3 for position 5 & 8). Thus, we assigned a higher frequency to the middle finger. The three frequencies selected

for the fingers were 480 Hz for the thumb, 600 Hz for the index finger, and 720 Hz for the middle finger. It was possible to match vibration transmissibility around -130 to -140 dB regardless of contact sites and fingers. We equally spaced the encoding frequencies to ensure that the effect of possible interferes between the frequencies should be balanced. For the other vibration parameters, e.g., amplitude and duration, we conducted pilot tests to minimize them to the levels where signal quality is acceptable. The duration was 50 msec, and the amplitude was 40 % of the maximum power of our transducer and amplifier pair.

How to Initiate Interaction

Interaction with the suggested input interface starts by making contact with an object or a surface of interest. The first requirement of the interface is to notice the contact, and most of the electronic devices already have the hardware, e.g., touch screen and button, to support such functionality. Our visionary aim is to deploy our interface to almost any rigid surfaces or objects having enough space to touch, including a monitor, a table, a medicine bottle, a door, and a light switch. Since such surfaces have no other way to recognize contact made by users, it is essential to detect the moment of contact on rigid surfaces with our recording platform Therefore, we implemented an algorithm for detecting tapping sounds at the recording platform.

The applying median filter has been a well-accepted solution to differentiate impulsive sounds from other slowly varying sounds [72, 73]. The basic idea is to compare an original power sequence and its median-filtered sequence since the median filter filters out a signal having less than half of a filter width. In

Figure 3.8, our median filter (filter width = 50 ms) follows up a power sequence when playing music and saying words (both approximately 15 cm apart from the recording platform); not for tapping sounds near our recording platform.

Our tapping detection algorithm iteratively observes the recent 150 ms power sequence for every 100 ms. After subtracting the power sequence and its median filtered sequence, the algorithm finds the index where the subtraction is larger than a threshold that was weighted by the amplitude of the median-filtered sequence at the moment. The detailed algorithm is presented in Algorithm 1.

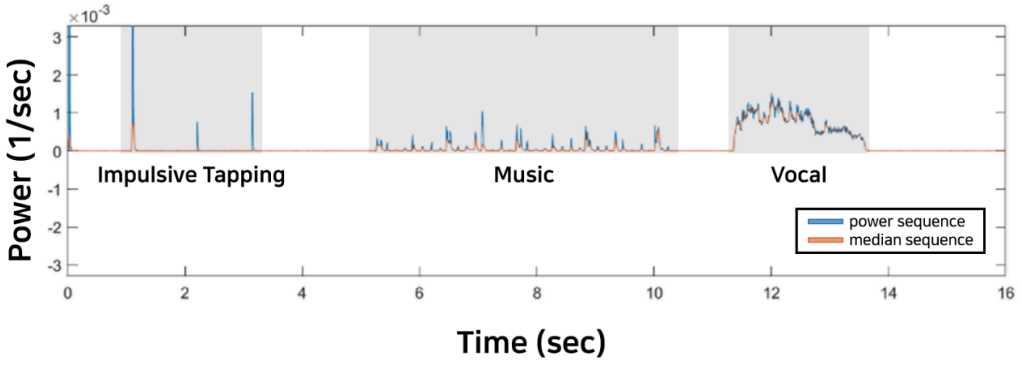

Figure 3.8: Sound samples from our recoding platform.

3.3.3 System Overview

Figure 3.9 illustrates a recording sample that an encoded vibration was propagated from the finger to the recording platform. Interaction is initiated by tapping on a surface. If the tapping is detected, our desktop operates its internal sound card to function as a data acquisition unit. Vibrations are executed at wearable rings, and a microphone starts recording. From the acquired sensor

Algorithm 1 Tapping Detection Algorithm

Require: a power sequence from input audio P, a median-filtered power sequence M, a threshold level for impulsive sound t_i, a median-weighted threshold t_m

```
1:  procedure TapDetect(P, M, t_i, t_m)
2:      idx ← indexof(abs(P − M) > t_i)
3:      if numel(idx) > 0 then                    ▷ impulsive sound detected
4:          idx_m ← min(idx)
5:          t_m ← M(idx_m) ∗ weight
6:          if P(idx_m) − M(idx_m) > t_m then     ▷ to reject voice and music
7:              Tapping Detected
8:          end if
9:      end if
10: end procedure
```

recording, we conducted a series of data processing to compute features for our classification method. For simplicity, we can directly examine encoded vibration frequencies for finger detection, but it was not robust to external noises and unexpected sounds. In the following section, we will explain how we discern contact finger(s) from the acquired signals in detail.

3.4 Evaluation

3.4.1 Data Collection

We recruited 11 participants (8 males and 3 females; 21-29.1 years old with M 25.4 and SD 2.6) for data collection. Participants were asked to wear our ring-type devices on the proximal phalanx of each finger, and they made contact with surfaces following the instruction from the experimenter. They only wear

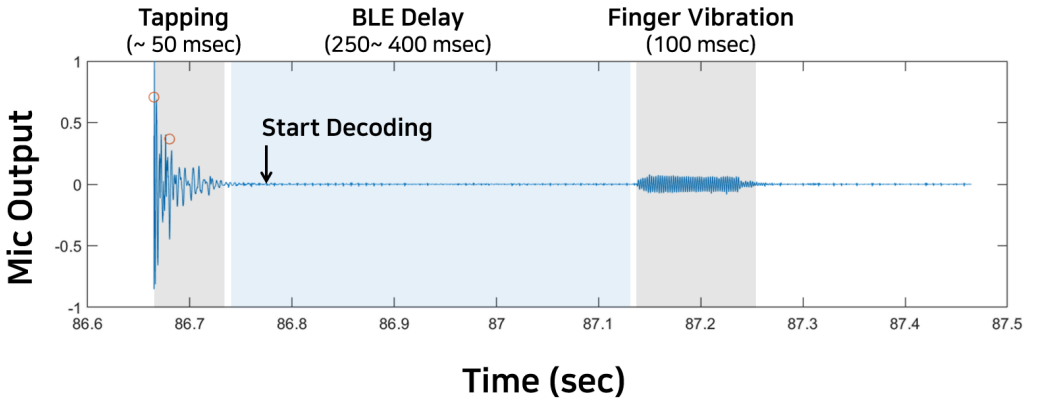

Figure 3.9: A recording sample from our system.

the ring devices on two fingers, changing the configuration of the rings depending on experimental conditions. In usage scenarios, we expect that leaving one finger free is better because it ensures the primary finger for interaction and avoids discomfort from being equipped with too many gadgets. All in all, there were three ring configurations (Thumb & Index (**TI**); Thumb & Middle (**TM**); Index & Middle (**IM**)) in this data collection experiment.

We collected data on the glass panel with our recording platform attached (Section 3.2.2) and the tablet (Section 3.2.3). For simplicity in detecting contact during this data collection, we exploited the touch interface of the tablet by using a TCP/IP connection and attached an IR touch panel to the glass panel. Once contact was detected, the internal sound card was operated as a data acquisition unit for a second, executing vibration signals and receiving microphone recordings concurrently.

For each surface, we divided a surface into several sections, and contact

conditions were defined from the section arrangements. The surface of the glass panel was divided into four quadrants where the center of the surface was aligned to the origin of the Cartesian coordinate. We attached the recording platform to the center. For each ring configuration, participants touched a quadrant for each single finger contact, and they made multi-finger contact twice within a quadrant. We repeated this twelve times because there were the three ring configurations (**TI**, **TM**, **IM**) and four touch sections. In total, each participant conducted 24 trials (2 *repetition* $\times$ 3 *ring configuration* $\times$ 4 *section*) respectively for the single (T,I, and M) and multi-finger contact (T+I,T+M, and I+M).

The touch area of the tablet was reallocated to the equally spaced 3 $\times$ 2 grid, as we did in Section 3.2.3. For the single finger contact, participants touched each grid section twice with the three different ring configurations, which resulted in 36 trials for each participant. From the 6 grid sections, there are 36 possible combinations for the multi-finger contact, but we rejected some conditions that are difficult to perform. Thus we found 19 same combinations for **TI** & **TM** and 11 combinations for **IM**. In summary, we collected 1463 trials of contact with vibration rings from 11 participants.

To examine the quality of data, we visualized the collected signals. Figure 3.10 visualizes the spectral information of all six contact finger conditions, and each plot presents noticeable differences in the detected signal frequencies. Hence we proceeded to further steps to build classification models.

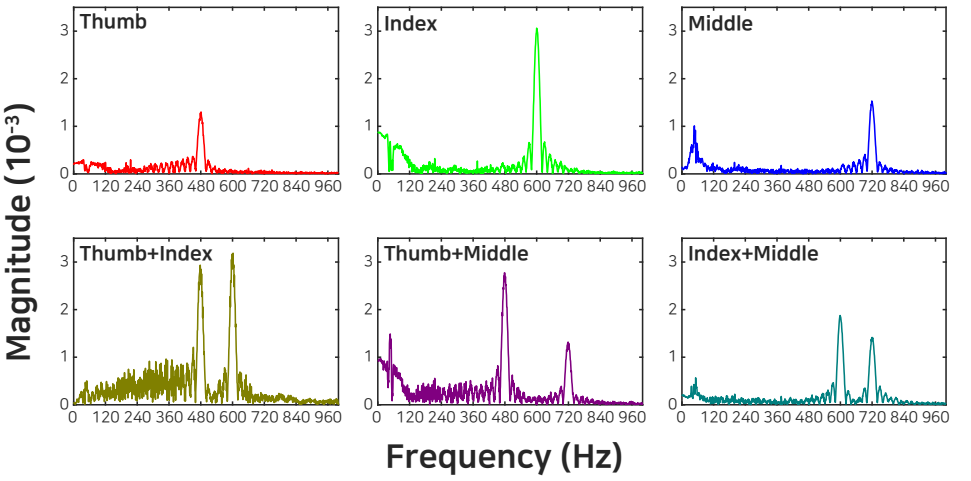

Figure 3.10: The spectral information of six contact finger conditions using FFT.

3.4.2 Preprocessing and Feature Extraction

The collected signals from the previous section were processed to extract features for classification models. We first designed a band-pass filter (BPF) to wipe out unnecessary spectral information. The BPF was a Chebyshev type-2 filter that has stopband frequencies 360 & 825 Hz, passband frequencies 400 & 750 Hz, and stopband attenuation level was 100dB. For each trial, we conducted a Fast Fourier Transform (FFT) where the frequency resolution was 1 Hz. For visualization, we plotted the distribution of the FFT magnitudes at the three encoded frequencies (Figure 3.11, left). The 3D plot presents grouped data points according to the six contact finger conditions, and the data looks well distributed depending on the contact finger conditions; however, there existed some ambiguities and overlaps around the origin of the coordinate.

For the next step, we normalized the FFT of each trial with its minimum and maximum values. This process stresses out the spectral information at featured frequencies, which also standardizes results collected from different surfaces and conditions. We found that this process actually spread the data over the 3D space (see Figure 3.11, middle).

We conducted the Principal Component Analysis (PCA) to characterize our data set. From this dimension reduction method, we can avoid using the full sequence of the normalized FFT or using features not enough to describe the data set. We applied PCA to the normalized FFT of all 1463 trials, and 91.87 % of the variance was accounted for by the first ten principal components. In the right plot of Figure 3.11, we visualize the distribution of the data set with the first three principal components explaining 41.65 %, 34.54 %, and 7.22 % of the variance, respectively. Finding optimal axes to describe the data set, the distribution of the first three principal components better explained our data set than that of the normalized FFT magnitudes at the three encoded frequencies.

3.4.3 Feature Selection and Classification

From a series of data processing, we extracted several features for classification in the previous section. We tested three classification methods: Probabilistic Approach (PA), Support Vector Machine (SVM), and Random Forest (RF). As a cross-validation method, we used a Leave-one-Person-Out (LOPO). If the performance of a classifier is measured by the method, the classifier is trained and tested by a set of data from different individuals. Therefore, the measured performance is an unbiased estimate of real usage contexts. For each iteration, data

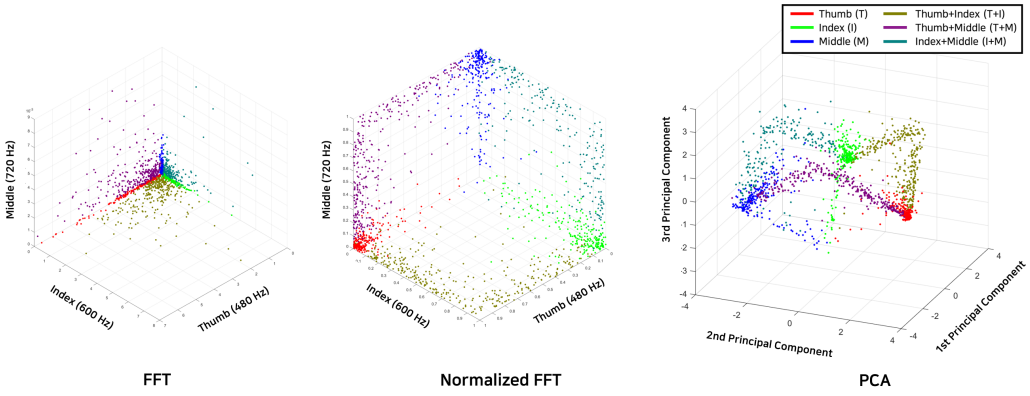

Figure 3.11: The three distribution of the collected data. From left to right, the raw FFT values of the three encoded frequencies, the normalized FFT values of the frequencies, and the first three principal components. Each distribution has six following groups: Thumb (T; red), Index (I, green), Middle (M, blue), Thumb+Index (T+I, olive), Thumb+Middle (T+M, purple), and Index+Middle (I+M, turquoises).

from ten participants trained a classification model, and data from the other tested to check the performance of the model. As for measuring performance from LOPO cross-validation, we measured mean accuracy and its standard deviation recall, precision, and computation time, which are summarized in Table 3.1 and Figure 3.13. The computation time is the average duration required to build a classification model and predict a single instance.

The first method, Probabilistic Approach, starts with the estimation of the probability distribution function (PDF). For each ring configuration (**TI**, **TM**, and **IM**), we collected three different contact conditions, which are two other single finger contact and one multi-finger contact. Therefore, we computed three PDFs each by maximum likelihood estimators of two-dimensional Gaussian distri-

bution. Unlike the other two classification methods, we used the FFT magnitudes without the normalization or PCA for simplicity (see Figure 3.11, left), and the classification performance of PA was the best with the feature set. As an illustration, all the data collected from **TI** were divided into three sets by different contact finger conditions, e.g., *T*, *I*, and *T+I*, and we computed three 2D Gaussian distributions. From each distribution, we calculated a probability of a new instance from a given PDF and then compared the three conditional probabilities to choose a distribution that resulted in maximum probability. As a baseline method, the mean accuracy of our probabilistic approach was 91.17±7.48 %, and the accuracies from each ring configuration were 92.46±3.21 % (**TI**), 94.58±4.4 % (**TM**), and 86.48±10.52 % (**IM**). In Figure 3.13, **IM** resulted in the lowest classification accuracy where multi finger contact by the index and middle finger classified as single finger contact of the fingers, which lowered the recall of *I+M* (78.95 %) and the precisions of *I* (83.87 %) and *M* (86.42 %). Compared to the other classification methods (see Table 3.1), the accuracy of this approach presented high variability depending on which data was used to train and test the classifier.

For SVM, we implemented a classifier with the LIBSVM library [74]. Since there are no constraints in the length of a feature vector for SVM and RF, we trained SVM classifiers to discriminate all six contact finger conditions. We first tested to find the optimal number of features selected from the principal components, and a set of features included principle components from the first to ascending order. In Figure 3.12, the mean accuracy of our cross-validation

Table 3.1: The Comparison of Classification Performances of LOPO Cross-validation with respect to Classification Methods and Features

	$PA_{Baseline}$	SVM_{TIM}	$SVM_{BandPass}$	SVM_{All}
Accuracy (Mean, %)	91.17	83.94	96.51	96.72
Accuracy (SD, %)	7.48	5.20	1.91	1.79
Time (Mean, ms)	99.24	0.05	1.17	63.74
	SVM_{10PC}	RF_{4PC}	RF_{10PC}	$RF_{BandPass}$
Accuracy (Mean, %)	96.04	95.22	94.53	93.92
Accuracy (SD, %)	1.90	3.18	2.63	3.34
Time (Mean, ms)	0.06	1.09	1.33	2.67

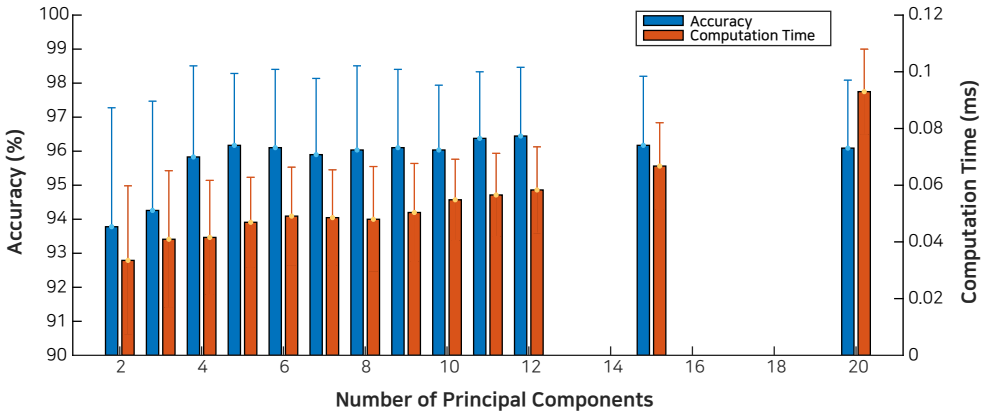

Figure 3.12: The performance measurements of SVM classifiers depending on the number of principal component features. The left axis presents for the mean accuracy (blue bars) and its standard deviations (blue error bars) of LOPO cross-validation models. The right axis is for the mean computation time (orange bars) and its standard deviation (orange error bars).

method reached an estimated plateau when more than the first four principal components were used as features, but the standard deviation of the classification accuracies presented the minimum value of 1.90 with the first ten. The computation time slightly increased by 0.013 ms when the number of the PC features increased from 4 to 10, but both the mean accuracy increased and its standard deviation decreased. Therefore, we continued to the next step for feature selection with the first ten principal components. Tested feature sets for SVM classifiers were the first ten principal components and the three subsets of the normalized FFT features. The three subsets included normalized FFT magnitudes at the three encoded frequencies (480, 600, and 720 Hz; TIM), the

frequencies around the band-pass filter range (400-800 Hz; BandPass), and all available frequencies (0-22050 Hz; All). These feature sets were fed to C-SVM with a linear kernel to train a classifier respectively. As denoted in Table 3.1, all SVM classifiers performed better than the baseline method with respect to all performance measures, except when only the three encoded frequencies were used to formulate a feature set. In our test, the PCA feature set was the best option because the SVM classifier built upon the feature set presented comparable mean accuracy without increasing the computation time. Although the SVM classifiers made from long feature vectors, BandPass (length = 401; accuracy = 96.51±1.91; computation time = 1.1 ms) and All (length = 22051; accuracy = 96.72±1.79; computation time = 63.7 ms), presented slightly better mean accuracies than that from the PCA features, their computation time were respectively 20 and 1078 times longer than the PCA feature classifier (length = 10; accuracy = 96.04±1.90; computation time = 0.06 ms). We found that the PCA feature classifier sometimes classified *I+M* as *I* or *M* and *T+I* as *I*, but no precisions were lower than 90 %, and all recalls were higher than 92 %.

Lastly, we trained a Random Forest classifier with PC features by using TreeBagger class in Matlab. From out-of-bag validation, the ensembles of twenty trees resulted in 6.15 % of the error rate, and we used the number for the trees of our RF classifier. When the first ten PC were used, the mean accuracy of the RF classifier (accuracy = 94.53±2.63; computation time = 1.3 ms) was a little lower than that of the SVM classifier built upon the same features (accuracy = 96.04±1.90; computation time = 0.06 ms). The RF classifier was not

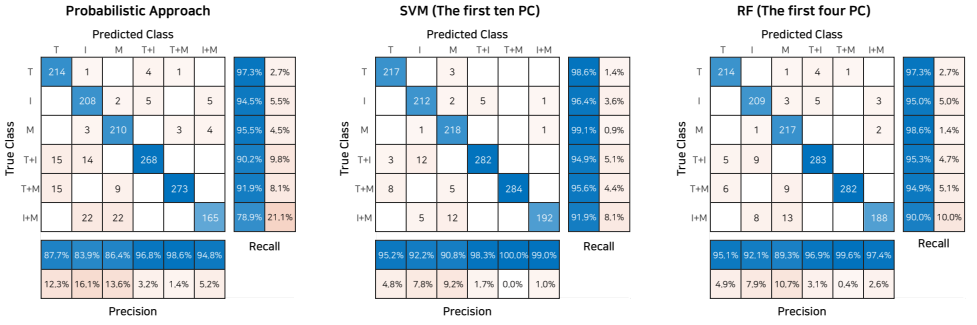

Figure 3.13: The confusion matrix of the classifier of each classification method. For each confusion matrix, the recall and precision of each class are presented.

robust to the variations in data sets and not as fast as the SVM classifier. To further improve the RF classifier, we observed a measure of importance for each feature, and the feature importance is the increase in prediction error when the values of a feature are permuted across the out-of-bag observations. The first four principal components presented more than 2 % of increases in error when they were rearranged across the validation set. Using the reduced number of PC features improved the performances of a new RF classifier (accuracy = 95.22±3.18; computation time = 1.1 ms), but not as good as the best SVM classifier. In Figure 3.13, we presented the confusion matrix of the selected classifier of each classification method.

3.4.4 Subjective Evaluation

During the data collection, we asked the participants to rate their perception and unpleasantness about presented vibration signals. Three subjective measures include the perceived intensity of vibration and sound and the unpleasantness of

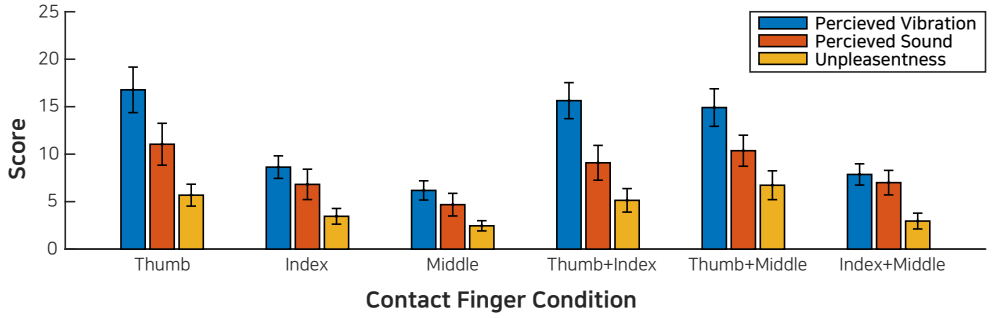

Figure 3.14: The mean scores of all subjective ratings. Error bars represent standard errors.

the signals. The participants verbally answered their ratings from 0 to 100, and a numeric scale with the descriptions about extreme points was presented for each measure. All measures were rated twice for each contact surface, and we pooled the data of the different surfaces. Figure 3.14 presents the mean values of all ratings received from all participants. The 480 Hz vibration assigned to the thumb is potentially presenting the most sensitive tactile sensation among the three encoded frequencies. The participants rated the perceived intensity of vibration and sound of T, $T{+}I$, and $T{+}M$ higher than the other contact finger conditions, but their mean values were still fairly low around 15. There were no noticeable difference between I and M. Also, none of the mean unpleasantness scores were over 7 out of 100.

3.5 Discussion

The idea behind the suggested input technique is simple, which is based on the analysis of vibration propagation. When contact is made between a user with wearable rings and a rigid surface with a microphone, the wearables execute vibration to be heard by the surface. Through the series of experiments to identify the expected pathways of vibration propagation, we figure out how to transmit frequency information to the sensor end. After several signal processing steps to extract a feature vector, a classification algorithm analyzes the features to decode a contact finger. Furthermore, we tackled the recognition of multiple simultaneous contact fingers also. As a proof of the concept, we implemented the hardware and algorithms, and the capability of vibration to notify contact fingers to rigid surfaces was validated. As a result, the SVM classifier trained from the ten principal components presented both fast (0.06 ms) and reliable (96.04 %) classification performance when trained and tested across data from different individuals.

We trained our classifiers with the data collected by two different surfaces. The frequency spectrum of the collected data was normalized to alleviate the difference between the two surfaces. From our validation experiment, we found no noticeable difference in classification errors between them. When tested the SVM classifier with the first ten PC, there were 30 misclassified instances from the tablet; 28 from the glass panel. We included PCA in our data processing pipeline, and the dimension reduction method was effective to characterize our data set with fewer dimensions. The reduced number of features decreased the

computation time without losing classification accuracy.

Our baseline method presented acceptable classification accuracy (90.17 %) with only three features. Its classification accuracy was under 90 % only for IM ring configuration, and the accuracy and its variability from the training and test sets significantly improved at the other two ring configurations. This probabilistic approach can be a good alternative when less computation is essential because it did not require some preprocessing steps. From the LOPO cross-validation, all classification methods did not result in many errors between single contact fingers. The single finger contact was not generally misclassified as the multi-finger contact, but most of the classification errors were from vice versa. *I+M* contact finger condition was the most error-prone (see Figure 3.13). Except for SVM classifiers, no other classifiers achieved over 90 % of the recall rate for *I+M* condition. It is reasonable to assume that SVM was the best classification method for our data set.

Our best classifier presented 96.1 % of recall rate when recognizing all six contact fingers; 98.0 % for the three single contact fingers and 94.1 % for three multiple contact fingers. We compare this performance with the performance of user-independent classifiers from previous research. The classification performance of our method is better than implicit methods where the accuracies of the same single contact fingers were listed as follows: 61.9-70.6 % (Gil et al. [53]; Capacitive Screen; RF); 70.9 % (Le et al. [54]; Capacitive Screen; CNN); 48.4 % (Becker et al. [57]; Electromyography; LSTM). Also, our method presented comparable performance when compared to the explicit method by Masson et

al. [63] (98.2-99.6 % for single contact fingers; 91.9-94.7 % for multiple contact fingers; Touchpad & Vibration Sensors).

Our system augments vibration on the finger. Although our participants answered pretty low on the unpleasantness score, it can be a limitation of our study if an application requires completely avoiding the tactile sensation. Except for such cases, we found a level of vibration that is strong enough to be detected as vibro-acoustic signals but not annoying. To minimize the tactile sensation, we recommend using frequency over 600 Hz to augmenting fingers with vibration. The perceived intensity of vibration and sound was rated twice (I and I+M; 600 Hz) to three times (M; 720 Hz) lower when contact finger conditions did not include the lowest encoding frequency (T,T+I, and T+M; 480 Hz), which resulted in around half in the unpleasantness score (see Figure 3.14).

Another limitation of our study is about frequency. Because it is almost impossible to test all frequency-finger pairs, we only tested a single frequency spacing (120 Hz) and carefully selected the three frequencies where the amplitude decibels were balanced. It is possible to detect more fingers by reducing the spacing between frequency, but the interference between two frequencies might take place when the frequencies get too close. Detecting more fingers can be beneficial because it means that such capability can be used to detect more fingers, even from another hand or person.

In the left plot of Figure 3.6, the vibro-acoustic transmissibility of our tablet lowered as frequency increases in general. From our experience, frequencies beyond 1 kHz were not detected well at the microphone end of the tablet. Although

the transmissibility of the earbuds was flat and simple, we expect that that is because of its simple structure. As the complexity of parts in an electronic device increases, it is difficult to estimate the transmissibility of the devices. This volatility in the vibration transmissibility of electronic devices is one limitation of our study. As a further study, the selection of vibration frequency can be adaptive to environment noise or device transmissibility to handle this limitation.

3.6 Conclusions and Future Work

The main focus of this study is to enrich the interaction possibility between users and everyday surfaces. Like projecting visual information on our body or surroundings in Augmented Reality, we try to augment fingers with vibration to make it communicate with surfaces or objects having a microphone. As a next-generation wearable, ring-type devices are versatile not just for notification but for many other purposes, such as activity tracking, wireless communications with other devices, and voice control [75, 76]. Assuming the usage context of the ring-type wearables, we have designed and validated a novel input technique that empowers everyday surfaces to recognize contact made by a vibratory-augmented finger. Starting from the investigation of sensing possibility, we processed vibro-acoustic signals out to train and test classification methods.

We can think of many further usage scenarios of this initial study. Since we embedded a microphone, it is possible to detect micro gestures, e.g., scratching and rubbing, after contact is confirmed. If it is available to decode many frequencies reliably, this system can also be extended to recognize contact from different

people or the other hand to enrich interaction. To distinguish more frequencies, we might intentionally generate interference patterns from different vibrations. We hope that this study envisions the usage of vibration to communicate with ordinary and mundane everyday surfaces.

IV. Identifying Static Objects by Visualizing The Propagation Dynamics of Vibration

4.1 Introduction

Living in the era of virtual reality, context-rich digital augmentation is an ultimate goal when coupling digital and physical worlds. Absence of comprehensive sensing methods, however, is one of the key obstacles against expanding the realm of digitally augmented computing. As such, previous studies explored ways for computing devices to recognize the context of use, e.g., location [7, 44], object [10, 9] and its state [77, 23], user's action [78, 10, 24, 43], and material [12, 79, 8, 9, 80], via numerous sensing technologies.

Since recognizing an object or its materials is beneficial to assume a user's context [7, 11, 12, 8], there have been numerous attempts to implement sensing methods for that purpose. The sensing methods exploit different physical channels, including photic, electromagnetic, acoustic, and vibratory, to amplify differences among a set of materials or objects. This physical channel of sensing determines the class of materials or objects that lead to reliable identification. Light-based sensing yields multi-spectral information that enables recognition of a variety of materials. However, this approach generally requires a flat surface for suitable light reflection. In addition, since only local information is retrieved,

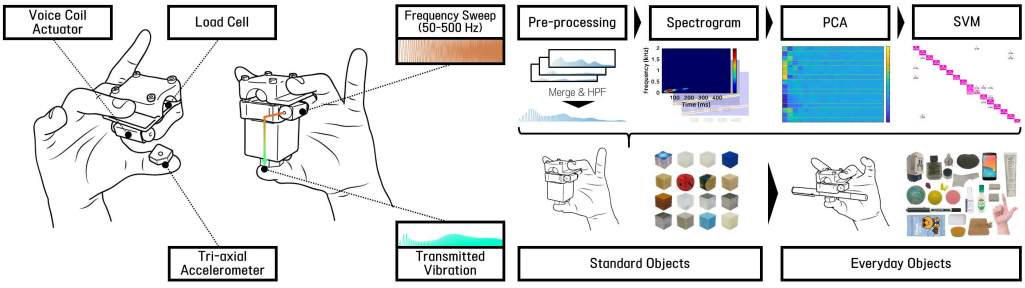

Figure 4.1: VibEye: system overview and operation principle (left). Data processing pipeline (right-top). A classification model is built from 16 standard objects and then applied to categorize 25 everyday objects (right-bottom).

light-based sensing does not ensure reliable recognition of the objects with complex material composition or arbitrary shape. Object recognition using electromagnetic signals is effective but only applicable to the objects that emit electromagnetic waves. Acoustic sensing focuses more on detecting the state changes of objects because acoustics waves are sensitive but weak.

In this chapter, we are concerned with distinguishing objects on the basis of their *material* differences exploiting the wave properties of vibration. As we often shake an object to feel its characteristics, we impose a frequency-modulated mechanical vibration to an object and then measure and analyze the response vibration. This approach allows us to deal with objects that have different mechanical properties, e.g., stiffness, damping, density, and weight. Such mechanical properties define the feel that users perceive when holding objects in hand, and our method is naturally tailored to tangible interaction.

As depicted in Figure 4.1, our hardware, named VibEye, is designed to support the pinching gesture holding an object between fingers. For accurate and

robust object recognition, we process the data in such a way that visualizes the spectral content of the object, which is determined by the material and structural properties, using a spectrogram. Spectrograms enable us to use standard image-based classification methods. We use PCA (Principal Component Analysis) in an unsupervised manner, followed by a C-SVM (Classification Support Vector Machine) classifier. This approach removes the cumbersome feature selection step for classifier design, which was an issue for prior vibration-based techniques.

We evaluated the VibEye system with two sets of objects: one consisting of 16 standard objects with the same cubic shape and the other with 25 everyday objects. The former was to stress their differences in the material, while the latter was to explore further applicability of our material-based recognition method to object with different shapes. When tested with 20 users, VibEye recognized the 16 standard objects with high accuracy (92.5%) in spite of uncontrollable hand orientation change and low-frequency motion. We also extend the classifier trained on the standard objects to the recognition of the unseen everyday objects to assess the extent to which material properties are captured in the classifier. The material-based classifier can indeed recognize everyday objects made of similar materials appropriately. Lastly, we showcase two interactive applications utilizing VibEye in virtual and augmented reality, respectively.

The main contributions of our work are with a proposal of a vibration-mediated recognition system of handheld objects emphasizing their material properties and a validation of its performance. VibEye's concept is useful for all tangible applications in real, virtual, and augmented environments.

4.2 System Design and Implementation

In physics, a mechanical wave propagates through the solid medium while oscillating and transferring energy. The vibration propagation dynamics depends on three mechanical components (mass, spring, and damper), and each of them is a function of vibration frequency. Materials with noticeable differences in such physical characteristics present distinct responses to the imposed vibration.

In our use scenario, a user grasps an object with two fingers, one wearing VibEye and the thumb (Figure 4.1, left). Then VibEye generates a short vibration, and it is transmitted to the thumb *through the object* and measured by an accelerometer fastened on the thumb's pad. From this I/O pair, we can estimate the vibration propagation dynamics of the object, and it may provide reliable information for object recognition. The vibration propagation dynamics is generally nonlinear, and its identification using the system theory is a quite complicated problem. Exploiting the fact that we trigger the object dynamics using a known input, we have designed a simple and effective data processing procedure. The input vibration also delivers confirmation feedback notifying proper and stable grasping for tangible interaction.

4.2.1 Hardware Design

VibEye is designed to support object grasping by pinching. Our 3D-printed prototype has a cube-like structure with a hole into which the middle finger is inserted like a thimble (Figure 4.2). Top and bottom parts are made separately and assembled using bolts and nuts. For vibration generation, a voice coil actua-

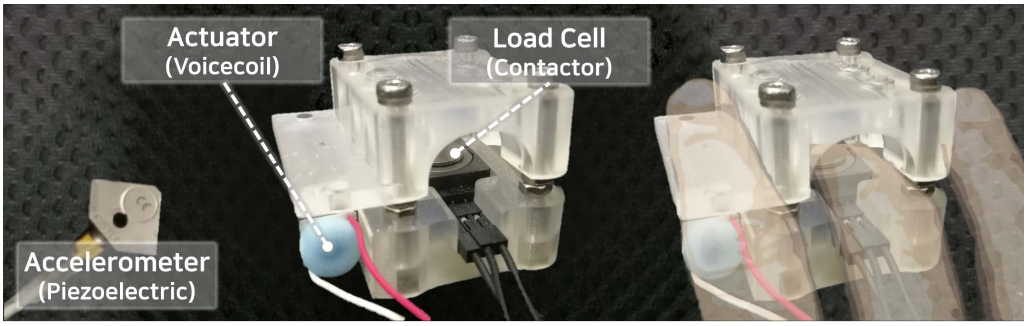

Figure 4.2: Hardware design of VibEye.

tor (Tactile Labs; Haptuator MM3C-HF), powered by an audio amplifier (Texas Instruments; TPA6211A1), is attached to the bottom part. A small compression load cell (TE Connectivity; FS2050-000X-1500-G) is also put inside on which the first phalanx of the middle finger is placed. This load cell is to measure active pressing force for contact detection and vibration trigger control. For the latter, we generate a vibration only when the measured pressure reaches 0.2 kgf for the regulation of operating condition. The vibration that has propagated through the object is sensed by a high-performance triaxial accelerometer (Kisler; Type8765A250M5) attached to the thumb's pad. All the sensors and actuators are connected to a data acquisition unit (National Instruments; USB-6251) with 20-kHz sampling rate.

4.2.2 Data Processing Pipeline

In general, the vibration propagation dynamics of an object is nonlinear. However, for a short period of time, it can be approximated by using linear dynamics. Our approach is based on this general linearization strategy.

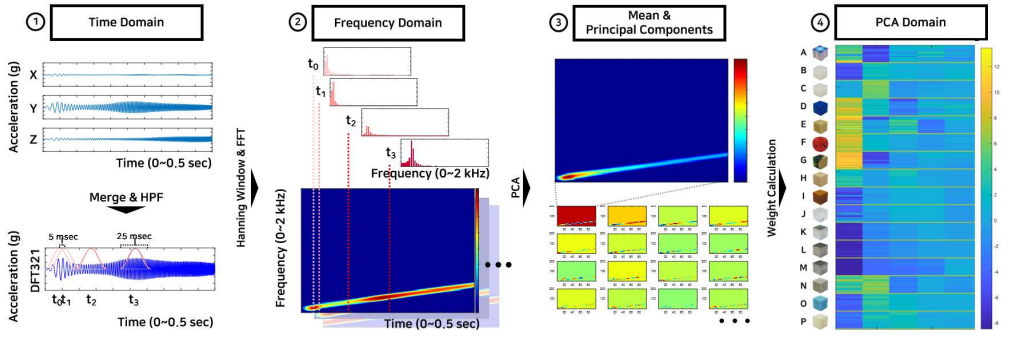

Figure 4.3: Computational procedure for signal processing and object recognition.

VibEye produces a sinusoidal vibration with the frequency varying linearly from 50 Hz to 500 Hz as an input to the object. This method is called sinusoidal frequency sweep, and it is widely used for system identification to trigger the response of a system in the frequency range of interest [81]. The frequency range was experimentally optimized for object recognition. The signal duration is 0.5 s, which is transient enough not to interfere with the user's gross motion and also sufficiently long for faithful dynamics reconstruction. The output vibration from the object is measured by the accelerometer. This I/O vibration pair is fed to a series of signal processing operations (implemented with MATLAB).

The vibration output is preprocessed as follows. First, we combine the three orthogonal signals from the triaxial accelerometer to make it invariant to the hand's orientation changes. We use the DFT321 method that maximizes both temporal and spectral similarity between the three individual signals and the merged signal [82]. This step may substantially improve the reliability of accelerometer information compared to the previous methods using individual sig-

nals separately [10]. Second, we apply a high-pass filter (HPF) to remove the effects of low-frequency hand motion. The bandwidth of human voluntary motion is very low, and that of the wrist motion for daily activities is about 5 Hz [83]. For HPF, we use a Chebyshev type-2 filter that has a flat passband with stopband frequency 5 Hz, passband frequency 50 Hz, and stopband attenuation level 100 dB.

Next, we compute the spectrogram of the preprocessed output signal, following the procedure shown in Figure 4.3. The output signal is 0.5-s long, and it is segmented to a sequence of 96 short signals by sliding a 0.025-s long Hanning window. Each segment overlaps 80% with the neighbors to preserve spectral continuity. Then, we apply 2048-DFT to every segment and stack the results along the time to construct a single spectrogram (96 by 1025). This raw spectrogram is filtered by removing the values lower than a cutoff level δ to suppress noise and transients, and then the outcome is normalized. The final spectrogram is unique to the object, like a *signature*, since we use the same input vibration to all objects (see Figure 4.4). This allows us to recover the mechanical characteristics of the object sufficient for recognition, without fully identifying nonlinear dynamics.

We collect spectrograms for various objects. Then, object recognition corresponds to classifying an input spectrogram into the spectrograms of the objects. To this end, we apply PCA to the spectrograms. PCA extracts the most discriminant features from the images in an unsupervised manner, and use the results for classification [84]. Therefore, we simply use a single image for classification, without defining and calculating many explicit features from the results of DFT

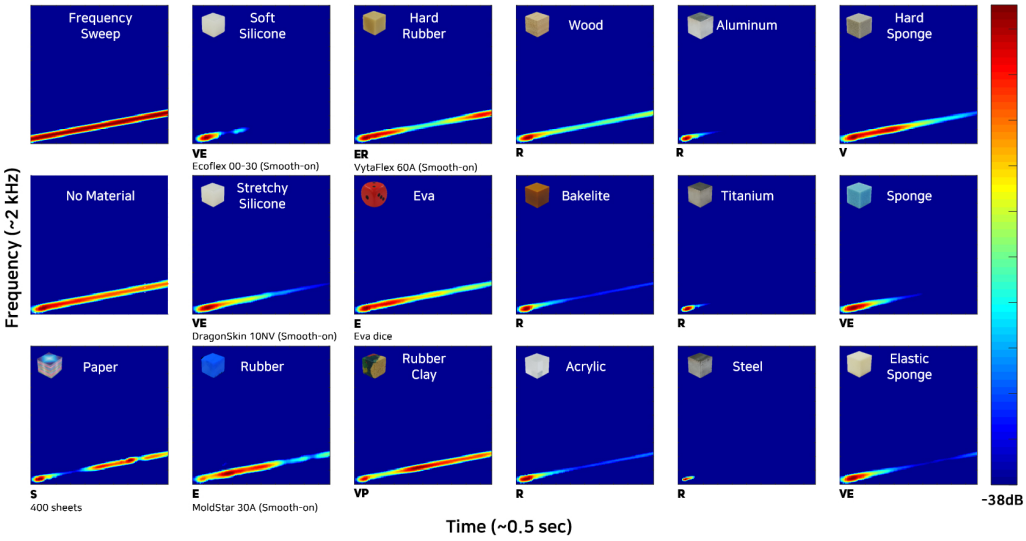

Figure 4.4: Spectrograms of 16 standard objects. Objects are marked with material properties (R: rigid, E: elastic, V: viscous, P: plastic, and S: stacked). The cutoff level δ was -38 dB. The cubic objects that we molded from liquid materials are specified with the material manufacturers and models.

as in the previous work [10, 41, 44]. As features for SVM, all the resulting PCs (principal components) of the spectrograms are fed to C-SVM (implemented with the LIBSVM library [74]) with a linear kernel to train a classifier.

The above procedure is simple and requires very little effort for tuning. The only critical parameter is the cutoff level δ for spectrogram computation, and the tuning results are easily distinguished by looking at the images.

4.3 System Evaluation

4.3.1 Sample Sets

Standard Objects

We prepared 16 cubes as shown in the insets of Figure 4.4. Their mechanical responses are independent of the vibration stimulation orientation (top-bottom, left-right, or front-back). We carefully selected 16 different materials to cover the diverse range of elasticity, viscosity, and weight of everyday objects. The edge length was 35 mm for all cubes, except for two slightly larger cubes of eva foam and paper. Using a variety of materials is important not only for the evaluation of object recognition performance, but also for affording rich haptic sensations to users who use the cubes as props—the 16 cubes work as basic building blocks for the feel of interaction. We call them *standard* objects, and their spectrograms are shown in Figure 4.4.

Everyday Objects

We also collected 25 *everyday* objects of complex shapes and material compositions (Figure 4.5). They represent casual objects that can be used for tangible interaction with natural affordance. They also encompass the various material properties of the standard objects and are sufficiently small to be held by pinching. Some of them are rigid and heavy (perfume, mobile phone, and multi-plug), rigid and light (spray, cosmetics, small table clock, wooden plate, and pen), packaged (wet glue, wet tissue, and toothpaste), heterogeneous (wash sponge and wrist pad), or homogeneous (wet sponge, small polyurethane (PU) ball, large PU ball,

synthetic rubber ball, jelly, elastic eraser, hard eraser, ear plug, and wristband). The rest are three human finger parts (the first phalanx of the thumb and the first and second phalanx of the index finger). Here we consider a scenario of using the thumb and index finger of the dominant hand for interaction while wearing VibEye in the non-dominant hand for object recognition.

4.3.2 Recognition Performance

We measured the response of each standard object 20 times using VibEye worn in *one* user's fingers and then processed the measured vibrations as described in Section 4.2. This step resulted in 320 spectrograms, and they were used as input images to PCA. The PCA results were reasonable (see the right panels in Figure 4.3). Nearly 0.1 million pixel information in each spectrogram is represented by 319 PCs. On average, the first PC explained 65.4% of the variance, and 90.7% of the variance was accounted for by the first three PCs.

We then ran cross-validation tests using C-SVM classifiers and obtained an accuracy of 96.9% and 96.3% for 5-fold and 10-fold cross validation, respectively. This high performance instantiates the effectiveness of our method. Hence, we proceeded to build a classifier to be used in our user study with many users, also including the 25 everyday objects. For that, we divided the dataset into two for training and testing while varying the proportion and tested the resulting classifiers with different users. The most balanced classifier was found at the 1:1 proportion with 94.4% accuracy, and this one was used for the user study.

The computation time of our object recognition method is also appropriate for tangible interaction. A single execution takes only 31 ms on average in Matlab.

Figure 4.5: Twenty-five everyday objects.

4.4 User Study

We conducted a user study in order to test the performance of VibEye with actual users. The classifier used was built from the data of one user, as described in Section 4.3. The first goal was to test whether the classifier can recognize the standard objects held in other users' hands. The second goal was to observe how the standard object classifier reacts to unseen everyday objects. Some of the 25 everyday objects and some of the 16 standard objects are composed from similar materials. If there is an everyday object consistently recognized as a certain standard object, it means that we can use the classifier to recognize that everyday object on the basis of material. This user study was approved by the Institutional Review Board (IRB) at the authors' institution (PIRB-2017-E068).

4.4.1 Methods

We recruited 20 right-handed participants (16 males and 4 females; 19–39.5 years old with M 23.5 and SD 4.18) for this user study. Each participant was paid 10 USD.

Participants put the VibEye device on their non-dominant hands. All participants finished two sessions, first with the 16 standard objects and the other with the 25 everyday objects. Also, each session had three repetitions. The presentation order of the objects within each repetition was fully randomized. The first repetitions were regarded as practice, and their data were not included in data analysis.

During the experiment, participants followed instructions shown on a monitor screen. The instructions were simple: hold an object by pinching and apply gentle pressure between the middle finger and the thumb so that it remains in the displayed force range (0.2 ± 0.02 kgf). After the contact pressure had stayed within the force range for 500 ms, a vibration was generated for frequency sweep. The accelerometer on the thumb picked up the vibration that had propagated through the object. Participants were asked to align the object's center of mass between the two grasping fingers while avoiding touching the object with other fingers or any other things around with the object. There were 48 trials for the session with the standard objects and 75 trials for the everyday objects. The experiment took less than an hour.

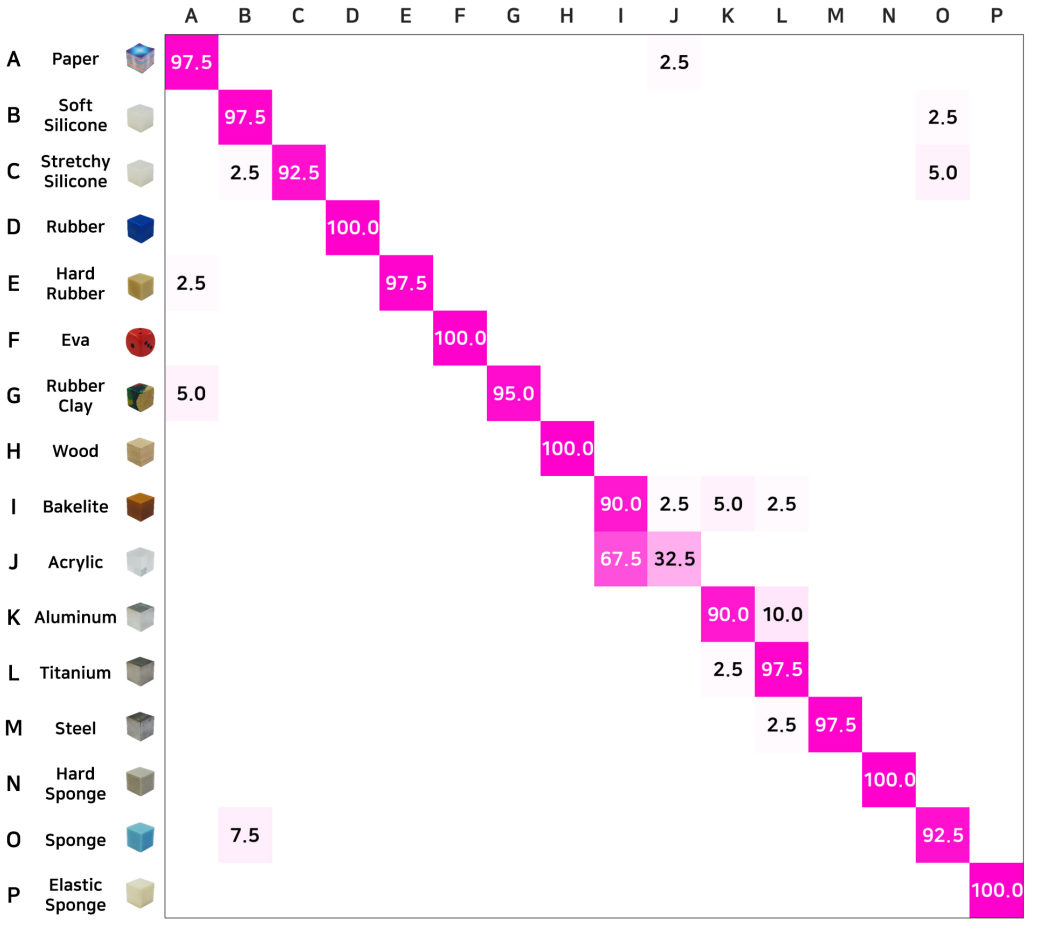

Figure 4.6: Confusion matrix for recognizing standard objects.

4.4.2 Results

Standard Objects

A confusion matrix for the standard objects is shown in Figure 4.6, where a number in the (i, j) cell indicates the percentage of the i-th object classified as the j-th object. It is evident that the diagonal terms are dominant for almost

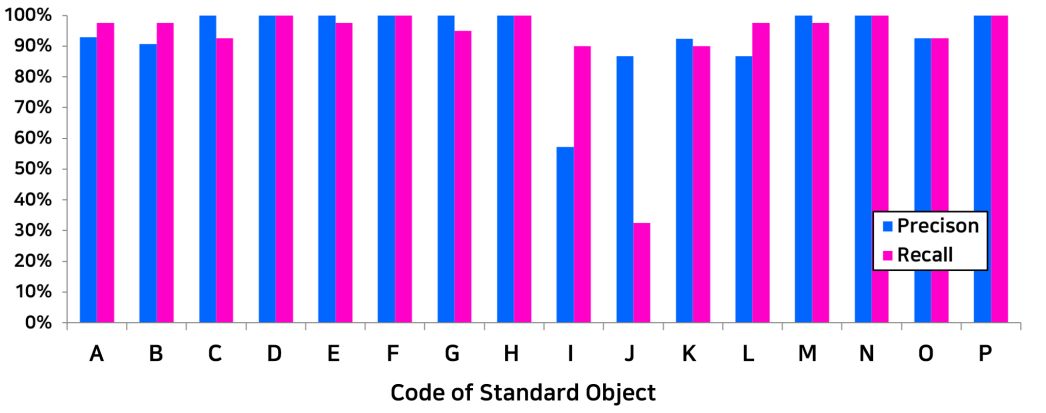

Figure 4.7: Precision and recall for standard objects.

all objects. The average accuracy over all standard objects and participants was 92.5%. This result validates the effective of our one-person classifier in recognizing the standard objects held by many different users.

The most noticeable errors were present with the acrylic cube that was recognized as the bakelite cube by 67.5% (Figure 4.6). These two rigid plastic cubes have similar mechanical properties (acrylic: density 1.19 kg/m^3, weight 50.8 g and bakelite: 1.3 kg/m^3, 59.9 g). Our method was unable to distinguish such subtle differences. When the two cubes' data are aggregated, the accuracy is improved to 96.9% (SD 3.8%).

Individual recall and precision values are shown in Figure 4.7 for all the standard objects. On average, precision was 93.7% (SD 11.0%), and recall was 92.5% (SD 16.4%)[1]. The average f-score was 92.0%. These statistics re-confirm the effectiveness of VibEye. Here again the bakelite (code I) and the acrylic cube (J) caused the performance drop. Combining the two cubes's data improves the

statistics to 97.0% (SD 4.4%), 96.9% (SD 3.2%), and 96.9%, respectively.

Everyday Objects

Figure 4.8 shows a confusion matrix of the everyday object classification results. Note that the two standard objects with very similar materials (bakelite and acrylic) are aggregated as plastics for simplicity.

We illustrate how to interpret the results in Figure 4.8 using examples. The cell at which "wet glue" and "G" are crossed represents that wet glue was recognized as rubber clay (code G; see Figure 4.6) by 80%. Similarly, the cell of "wet glue" and "A" tells that wet glue was also identified as paper (code A) by 20%. Examining the individual cells this way allows us to summarize prominent mappings from everyday object to standard object, as shown in Table 4.1. If an everyday object was classified as a standard object with over 70% of ratio, that pair is enrolled in the table with their common mechanical properties. Eighteen everyday objects (out of 25) were paired.

Some of the everyday objects are elastic, and most of them are classified into one of the two silicones (B and C), rubber (D), and eva (F), as shown in the top group of Table 4.1. The specific relations are in agreement with their level of elasticity. In the middle group, wet (liquid) glue shows slow restoration after deformation due to its viscous content, and it is 80% classified as the most viscous standard object, rubber clay (G). The everyday objects in the bottom group are all rigid. They are paired with rigid standard objects with a reasonable

[1]The average recall is identical to the average accuracy because the numbers of presenting each object were all the same.

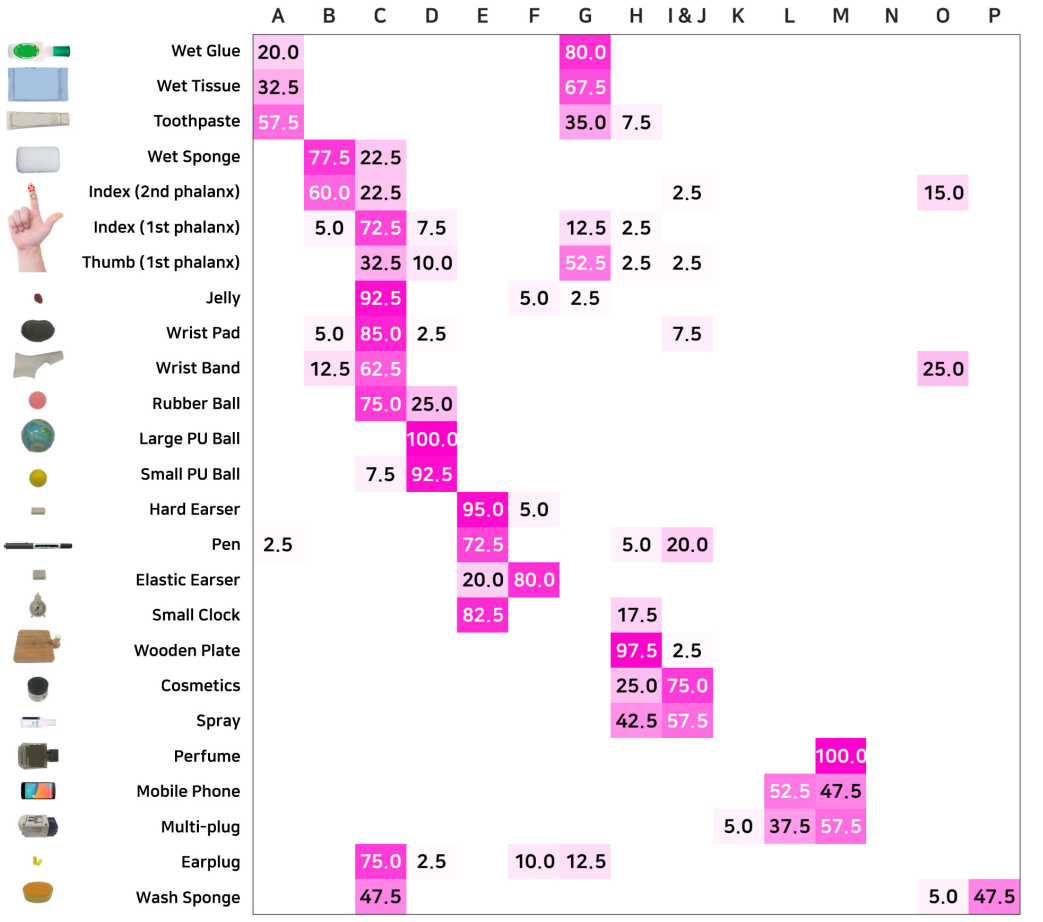

Figure 4.8: Confusion matrix for categorizing 25 everyday objects to 16 standard objects.

distribution. Weight is an influential factor to our classifier model, and heavy objects over 100 g (mobile phone, multi-plug, and perfume) are categorized to the standard objects made of metals (titanium (L) and steel (M)). Light and rigid objects are mapped to hard rubber (E) if they exhibit some noticeable properties, e.g., bouncing a bit when thrown (hard eraser) or making buzzing

Table 4.1: Prominent mappings from 18 everyday objects to standard objects (from Figure 4.8).

Everyday Objects	**Standard Object**	**Features**
Wet sponge	B (soft silicone)	Elastic and viscous
Jelly; wrist pad; index (1st Phalanx); rubber ball; earplug	C (stretch silicone)	Very elastic and viscous
Two PU valls	D (rubber)	Highly elastic
Elastic eraser	F (eva)	elastic and little viscous
Wet glue	G (rubber clay)	viscous
Wooden plate	H (wood)	Wooden and rigid
Hard eraser; pen; small clock	E (hard rubber)	Light and rigid (Little elastic or buzzing)
Cosmetics	I & J (plastics)	Light and rigid
Mobile phone; perfume; multi-plug	L & M (metals)	Heavy and rigid

noise from assembled parts (pen and small clock). Other light rigid everyday objects are classified to wood (H) or plastics (I & J), mostly depending on their materials.

4.5 Discussion

4.5.1 Summary of Results

Our work is based on a simple idea: when a user holds an object between fingers, we can recognize the object by triggering a short vibration and sensing the transmitted vibration changed by the object's mechanical properties. Our method empowers ordinary objects to work as props of rich haptic sensations,

contexts, and affordance for tangible interaction in any real, virtual, or augmented environments. For proof of the concept, we designed and implemented a simple prototype named VibEye and effective, efficient, and easy-to-use object recognition algorithms capitalizing on spectrograms and PCA.

We trained an actual classifier of the 16 standard objects on the data measured from one user. All the standard objects were of the same shape (cube), so the classifier learned their material differences. The classifier showed high cross-validation performance. When tested with 20 other users, the one-person classifier showed quite high performance (accuracy 92.5% and precision 93.7%). This is evidence of the capability of our method handling individual differences, e.g., different hand size and weight, and time-varying factors, e.g., hand orientation change and low-frequency motion. In another experiment where the 25 everyday objects with different shapes and materials were used, we conducted the experiment with the classifier built on the standard objects. This was to see how the material-based classifier reacts to the everyday objects of different shapes but similar materials. The one-person material-based classifier could find many good matches between the everyday and standard objects. Therefore, depending on objects used, material-based classifiers may suffice for accurate and robust object recognition, without training classifiers every time for new sets of objects.

When very high recognition accuracy is crucial, we can build individual models for each set of objects. Such classifiers are trained on both the materials and shapes of objects. For example, we trained a C-SVM classifier to the 20 participants' data of the 25 everyday objects with a cutoff level $\delta = -60$ dB. The

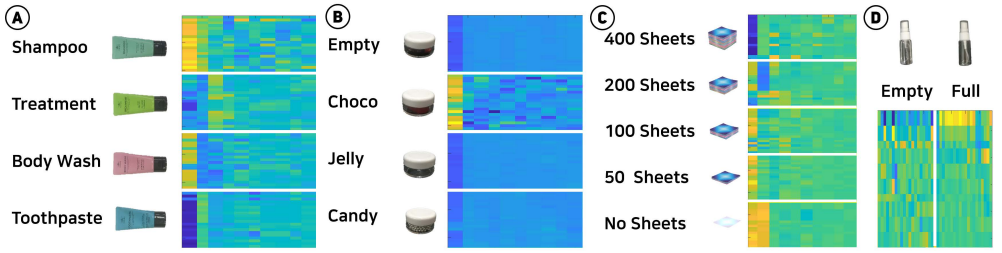

Figure 4.9: Another four sets of everyday objects and their PCA results (20 repetitions each): (A) Liquid body products in soft tubes, (B) candies in hard containers, (C) stacked papers, and (D) a spray bottle (empty or full).

recognition accuracy was as high as 93.1%. Moreover, we tested our method with the four sets of objects shown in Figure 4.9. They were liquid body products in soft tubes, candies in hard containers, stacked papers, and empty or full spray bottles. The recognition accuracy was nearly 100% for all the four sets. These four sets of objects are very difficult to recognize with other methods using vision or sound.

4.5.2 Hardware Improvement

Our prototype of VibEye is a bit bulky and not designed optimally for ergonomics; we rather focused on the function for proof of the concept. As such, its design can be improved in many ways by using other actuators and sensors. For example, there exist flexible thin-film vibration actuators that can be attached to the skin [85, 86]. Likewise, commercial film-type pressure sensors (e.g., those from Tekscan, Inc.) have been available for a long time. For accelerometers, tiny ones have recently been developed (approximate size 1 mm $\times$ 1 mm $\times$ 0.8 mm

[87]). Using such advanced actuators and sensors is likely to allow for a design of smaller, lighter, and more ergonomic hardware. However, the requirement of vibration transmission and sensing between fingers might still have fundamental interference with the normal use of fingers during interaction. This issue can be addressed more carefully after we build an improved hardware of VibEye.

Though the highest frequency we use is 500 Hz, the vibration output can have higher frequency due to nonlinearity or harmonics (e.g. candies inside a container). Therefore, we set our sampling rate to 20 kHz to ensure reliable measurement. However, the spectrograms in Figure 4.4 did not show significant energy above 500 Hz. Hence, 5–10 kHz sampling rates seems to be sufficient for spectrogram construction[2].

4.5.3 Vibration as A Sensory Cue

VibEye makes sound and vibration for object recognition, and they are perceptible. For some applications, we can *design* sound and vibration so that users accept them as adequate sensory feedback while the vibration still includes sufficient spectral information for building a spectrogram. There exists a plethora of literature even for vibrotactile effect design (e.g., see reviews in [89, 90, 91]). Our current implementation presents pleasant sensations to users. However, our method is inappropriate for the applications that disallows any sound or vibration other than those resulted from natural contact. It is a fundamental limitation of our approach that leverages structured mechanical vibrations.

[2]In practice, sampling rate for digitizing must be higher than 10-20 times of the highest frequency of interest of an analog signal [88]. Otherwise, important information is lost during analog-to-digital conversion.

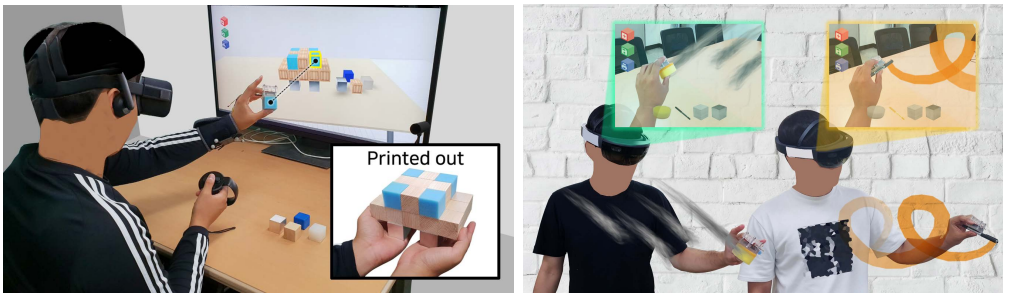

Figure 4.10: Applications of VibEye: (left) VR 3D modeling and (right) AR drawing tool.

4.6 Applications

VibEye allows tangible props to self-illustrate computing contexts in a simple and direct manner. The unlocked possibilities enable the design of digital environment that encompasses the afforance and experiences of the real world. VibEye also enables the unique haptic properties of real world objects, leading to rich tangible interaction. Delicate and assorted feels from the objects can be mapped to the functions and characteristics of user interface. Under these visionary design criteria, we have designed and implemented two applications, and they are presented in the rest of this section.

4.6.1 3D Modeling Interface for VR

Using blocks for 3D modeling is a popular paradigm (e.g., Minecraft and isometric toolkits in Unity). We can instill tangibility into such block-based modeling by using our 16 standard cubes as props (Figure 4.10, left). A user can design a 3D model by manipulating the cubes of desired materials with VibEye,

and the corresponding virtual blocks attain those materials. This function affords an authoring environment of highly congruent manipulation and representation. The 16 tangible cubes not only behave as haptic proxies [92, 93], but also provide diverse haptic sensations that are copied to the 3D model. Additionally, measuring the user's pinching force enables to distinguish whether the grasping is a mere grip, a request to identify the cube, or a command to insert the corresponding virtual block into the model.

Our 3D modeling application can be used with a tool that transforms multi-block models to CAD models [94]. Then the result can support material-rich 3D printing; its needs have been consistently raised in the literature [95]. Hence, our tangible 3D modeling interface has implication to 3D printing of diverse viscoelastic materials [96] and estimating the responses of elastic objects to be printed [97].

4.6.2 Drawing Interface for AR

In this application, a user puts on an optical see-through HMD and draws in a 3D space while holding an object in the hand wearing VibEye (Figure 4.10, right). The hand is tracked by a 3D tracker, and its trajectory is colored using AR. So the user can see both the real environment and the virtual drawing. Objects can be anything, e.g., a pen, sponge, finger, and eraser, but those with natural affordance and salient material properties are more adequate. Such tangible objects not only indicate functions (determined by the object identity), but also the textures of virtual drawing (represented by the object texture). Using this tangible input, we transfer the visual and haptic analog experiences to the digital

domain, also enabling other users to see and feel the saved drawings. In particular, depending on the haptic interface used, we can render different haptic properties such as texture, elasticity, and friction. For example, imagine a user holding a smartphone so that the user can perceive the haptic textures of drawing through vibration feedback.

4.7 Conclusions

In this chapter, we have presented VibEye, a system for vibration-mediated object recognition. VibEye is simple: its hardware requires only a vibration emitter and a sensor, and its software processes the data using well-defined image-based methods. Essentially, VibEye transforms the object recognition problem to an image classification problem. We have validated the effectiveness of VibEye in several ways, using the cross-validation results for the standard objects of the same shape but different materials, and recognition performance for other users' data and other unseen various everyday objects' data. Also demonstrated are the two tangible applications that capitalize on the advantages of VibEye.

We envision tightly-coupled virtual and real environments that are seamlessly controlled by tangible objects. We hope that the concepts embodied by VibEye could pave the way.

V. Investigating Effects of Contact Force and Vibration Frequency on Vibrotactile Sensitivity

5.1 Introduction

Humans require precise force control to execute fine manual tasks, which is generally facilitated to the great extent by providing adequate feedback. To design appropriate vibrotactile stimuli for manual tasks, it is essential to quantify human vibrotactile sensitivity over a large range of contact forces. In this chapter, we report the psychophysical detection thresholds for vibrotactile stimuli measured for five pressing forces that cover the range of forces encountered during ordinary manual tasks.

Although there has been extensive research on vibrotactile perception (e.g., [98, 99, 100, 49, 101, 102, 103, 104, 105]; also see [45] for review), only few studies addressed how contact force affects the perception. In most previous studies[106, 100], pressing force was controlled in a passive and static manner, and the ranges of force were relatively narrow and low. Recently, Papetti et al. [50] performed an experiment to measure detection thresholds for 250-Hz vibrations over a wide and high range of pressing forces (1.9, 8, and 15 N). Unlike the other previous studies, participants had to control their pressing forces *actively* to target values. The measured absolute thresholds decreased as the pressing

force increased.

In addition to the scientific knowledge provided by those previous endeavors, we need to describe the vibrotactile sensitivity of fingertip over a wide range of contact force sampled at intervals. We also need to take into account both of two mechanoreceptive channels of the PC channel and the RA(rapidly adapting)-I channel (NP-I channel) that are responsible for the perception of different temporal tactile properties. Therefore, we designed a psychophysical experiment with five pressing force levels (0.2 N, 2.0 N, 4.9 N, 7.8 N, and 10.8 N) and two vibrotactile frequencies (40 Hz and 250 Hz). Compared to the study of Papetti et al. [50], we also included a low frequency vibration stimulating the RA-I channel.

The experimental results showed stark contrasts between stimulus frequencies, depending on actively exerted pressing force. The detection thresholds for 40 Hz stimuli first increased then decreased as the pressing force increased, but the detection thresholds for 250 Hz stimuli generally decreased as the force increased. These results have immediate consequences on the design of vibrotactile feedback for manual tasks in many applications of tangible interaction, tele-operation, and VR.

5.2 Methods

This experiment was conducted under the protocols (PIRB-2017-E068) approved by the Institutional Review Board at Pohang University of Science and Technology.

5.2.1 Apparatus

We implemented a hardware system (Figure 5.1) to measure absolute thresholds accurately for a wide range of pressure levels. A commercial mini-shaker (Brüel & Kjær; Model 4810) was connected to a power amplifier (Brüel & Kjær; 2718), ensuring high precision and repeatability in a wide bandwidth (DC to 18 kHz). A load cell (Minebea; CB17-2K) with a dynamic strain amplifier (Senstech; ST-AM100) was placed under an acrylic cylindrical contactor (area 1.45 cm^2; height 0.5 cm) to measure the normal force. A participant put the index finger of his/her dominant hand on the contactor while placing his/her elbow on an arm rest. The shaker and load cell were assembled with an acrylic connector (7 cm × 4 cm × 1 cm) and were connected to a 16-bit data acquisition unit (National Instruments; USB 6251). A computer controlled the data stream at 10 kHz sampling rate. We developed an experimental program using Matlab Guide.

Before conducting the experiment, we carefully calibrated the shaker following the steps presented in [102]. The procedure was to identify linear input-output relationships for our apparatus at two stimulation frequencies. The shaker output was measured with a high precision accelerometer (Kistler; 8765A250M5) attached on the contactor. With the assembly parts (134 g) and the load cell (40 g) on the shaker, we measured the relationship between input voltage amplitude and output vibration amplitude at each frequency while the contactor was pressed by the finger. We calibrated the system with the five external pressing forces to compensate for the effects of finger loading on threshold measurements. The measured data in each condition were fit to a straight line without intercept

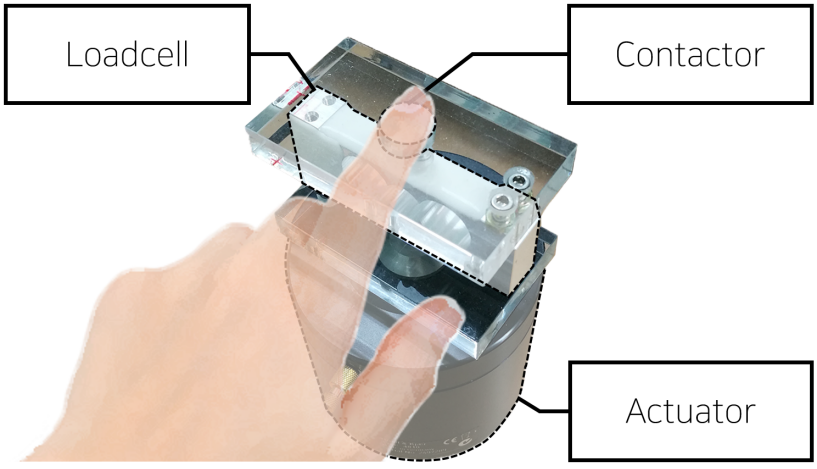

Figure 5.1: Experimental setup.

for linear interpolation ($r^2 > 0.97$).

5.2.2 Participants

We recruited ten participants (seven males and three females; 19 to 29 years old with a mean age of 23.9 years and standard deviation of 2.8 years) for this experiment. The participants reported that they were in normal health, i.e., without any known sensorimotor impairments or musculoskeletal diseases. All participants demonstrated normal ability to perceive vibrations in a practice session. Each participant was paid 15,000 KRW/hour (about 14 USD/hour) after the experiment.

5.2.3 Stimuli

The stimuli used in the experiment were sinusoidal vibrations generated by the shaker system. The vibrations had two frequencies: 40 and 250 Hz. The area

of contactor was 1.45 cm^2. All participants could cover the entire contact area with their index fingers even at the lowest pressure level (0.2 N). This area is large enough for the spatial summation of the PC channel to saturate (around 1.5 cm^2 [45]). The duration of vibrotactile stimuli was 1 s, which was sufficiently long for stable perception considering the temporal summation of the PC channel [45, 98].

5.2.4 Experimental Conditions

The experiment had a two-factor (pressing force × frequency) within-subject factorial design. The independent variables were pressing force (***Press***, 5 levels) and vibration frequency (***Freq***, 2 levels). ***Press*** represents the force exerted on the skin when a participant actively pressed the contactor with his/her index finger. ***Press*** had five levels: 0.2, 2.0, 4.9, 7.8, and 10.8 N. These values were selected to include the contact force levels for general haptic-based computing interfaces. This range also allows for comfortable pressing during interaction. According to Didomenico et al. [107], the maximum peak forces exerted by the index finger while pressing had a mean and a standard deviation around 40±15.2 N. The maximum force (10.8 N) used in our experiment is less than 1.92 standard deviations from the mean maximum peak force, thus it is accessible to more than 97.3% of the general population. We also confirmed that the maximum pressing force was not difficult to sustain and repeat. In contrast, the minimum force (0.2 N) represents the natural contact condition with a vibration source. Cholewiak et al. reported that 0.29 N (0.03 kgF) of contact force results in 1.4 cm^2 of contactor area [108], and it was regarded as a typical finger contact force in

psychophysical studies on vibrotactile stimuli [99]. Our minimum force of 0.2 N was also determined in a pilot experiment.

Freq had two frequency levels of 40 and 250 Hz. Research on cutaneous perception revealed that the dominant neural processing channels of 40 and 250 Hz vibrations are the RA-I and PC channel, respectively [45]. Hence, the two frequencies are good representatives for studying the effects of pressing force on vibrotactile sensitivity.

Participants finished a total of 10 experimental conditions (5 ***Press*** levels $\times$ 2 ***Freq*** levels). To alleviate transfer, learning, or fatigue, the presentation order of ***Freq*** was counterbalanced across participants using a Latin Square, and that of ***Press*** was randomized for each participant. Each experimental condition was presented to each participant only once.

5.2.5 Task and Procedure

An absolute threshold for each experimental condition was measured using the one-up two-down adaptive staircase procedure with two-alternative choices. Prior to the experiment, participants were provided with verbal and written instructions. Then, participants were asked to adjust settings (e.g., armrest position, chair height and leaning angle, contactor position, and keyboard position) to their comfort. Participants were also instructed to use their dominant hands to touch the contactor on the shaker and their non-dominant hands to enter responses using the keyboard. Participants wore earplugs and headphones through which 50 dBA white noise was played to block the noise and faint sound emanating from the shaker. Visual instructions were displayed on a computer monitor

to guide participants. There was a practice session before the experiment. Participants experienced initial ten trials from all the ten experimental conditions (all combinations of ***Freq*** and ***Press***) to become familiar with the stimuli and experimental procedure. The practice session lasted approximately 10 min.

The main experiment included ten sessions for the ten experimental conditions. During each trial consisting of two intervals, the target pressing force and current pressing force applied by the participant were visually displayed as two parallel slider bars on the monitor. In each interval, participants had to maintain the pressing force for longer than 0.5 s within a tolerance of ± 0.098 N for the 0.20 N force level and ± 0.29 N for the other force levels. Once the pressing force criterion was met, a 1 s long vibration was presented by the shaker. One randomly-selected interval contained the test stimulus, while the other interval presented no stimulus. After the two intervals, participants pressed the corresponding number key (1 or 2) to select the interval (first or second) in which they perceived a stimulus, and then hit the space bar to confirm their selection. Participants had to make their best guess when they were uncertain of the interval containing the stimulus (forced choice). Correct-answer feedback was provided visually on the screen during the experiment.

After each trial, the stimulus amplitude was changed following the one-up, two-down rule by a certain step size. That is, the stimulus intensity was decreased after two consecutive correct responses and increased after one incorrect response. This rule leads to the estimation of an absolute threshold with 70.7%-correct probability [109]. If the stimulus amplitude changes from increasing to decreasing,

or vice versa, it is said that a response reversal has occurred. The step sizes were designed to balance between fast convergence and fine resolution. The step size was initially 4 dB and was reduced to 1 dB after the third reversal. There was five-percent randomization in the initial stimulus amplitude for each session. The initial stimulus amplitude was set approximately four times higher than the expected thresholds measured in pilot experiments. Each session was terminated after nine reversals at the 1 dB step size.

Participants could take a break whenever they wanted. We forced participants to take a 30 s break between sessions and to rest after 10 min from the last break during a session in order to prevent fatigue and tactile adaptation. A single experiment lasted approximately 90 min (78 to 132 min), including all breaks.

5.2.6 Data Analysis

All threshold data were represented using peak displacement, which was converted from accelerometer measurement [110]. To obtain a threshold estimate, we averaged the stimulus intensities used at the last nine reversals in each staircase. These estimates of individual participants were averaged again for yielding the final absolute threshold. We also performed apparatus calibration under finger-loaded conditions, which generally showed lower peak displacement for the same input voltage. Three participants performed 30 repetitions of pressing the shaker in each of the 10 experimental conditions (2 frequencies and 5 pressing forces) from 0 to 1.2 V in 0.04 V intervals, and the resulting vibrations were measured. These data were used to derive linear input-output relationships for the loaded conditions. The thresholds were then converted to obtain absolute thresholds un-

der finger loading, and these thresholds are reported in the rest of this chapter.

We also conducted an in-depth analysis on the controllability of pressing force. The pressing force data from twenty equally-sampled data points collected during 1 s stimulus were averaged. The controllability of pressing force was characterized in terms of accuracy and precision.

All statistical tests were conducted using SAS (V 9.4) with the significance level α of 0.05.

5.3 Results

5.3.1 Absolute Threshold

Absolute thresholds for the sinusoidal vibrotactile stimuli delivered to the index fingertip are shown in Fig. 5.2 as a function of pressing force. Error bars show standard errors. For each pressing force, the detection threshold for 40 Hz vibration was higher than that for 250 Hz vibration. Furthermore, for the 40 Hz vibrotactile stimuli, the absolute thresholds increased until pressing force increased to 2.0 N, and the thresholds subsequently decreased as the pressing force increased further. In contrast, the absolute thresholds for 250 Hz vibration decreased and then increased as the pressing force increased, showing a V-shaped curve with the minimum at 7.8 N.

To confirm the validity of these observations, we performed statistical tests, starting with two-way repeated measures ANOVA with the independent factors of ***Freq*** and ***Press***. The sphericity assumption was not violated when tested by Maucly's test ($W = 0.132$, $p = .099$). Both ***Freq*** ($F(1, 9) = 69.21, p < .0001$)

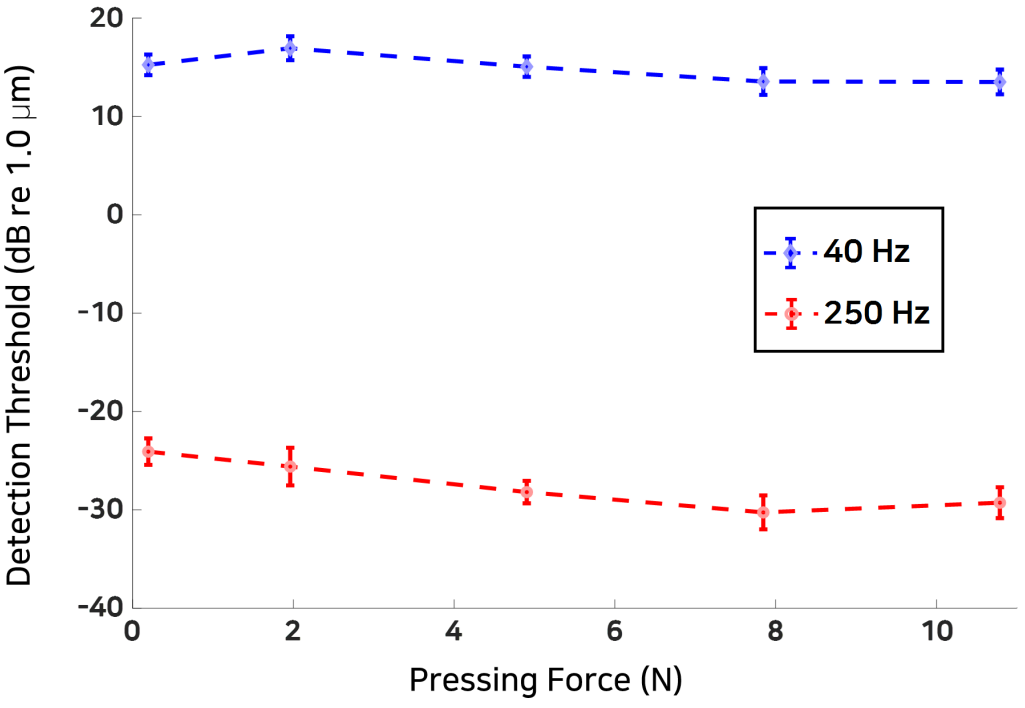

Figure 5.2: Absolute thresholds in terms of peak displacement in dB measured in all experimental conditions. Error bars show standard errors.

and ***Press*** ($F(4, 36) = 3.33, p = .0203$) had statistically significant effects on the absolute thresholds. The former allows us to state that the absolute thresholds were lower for 250 Hz vibration than for 40 Hz vibration. This is consistent with the well-accepted data and theories in tactile perception [45, 105].

The interaction between ***Freq*** and ***Press*** was found to be statistically significant ($F(4, 36) = 3.21, p = .0238$). For further inspection, we conducted simple effects tests on both factors.

First, at each ***Press*** level, the detection threshold for the 40 Hz condition was significantly higher than that for the 250 Hz condition (Figure 5.2). The

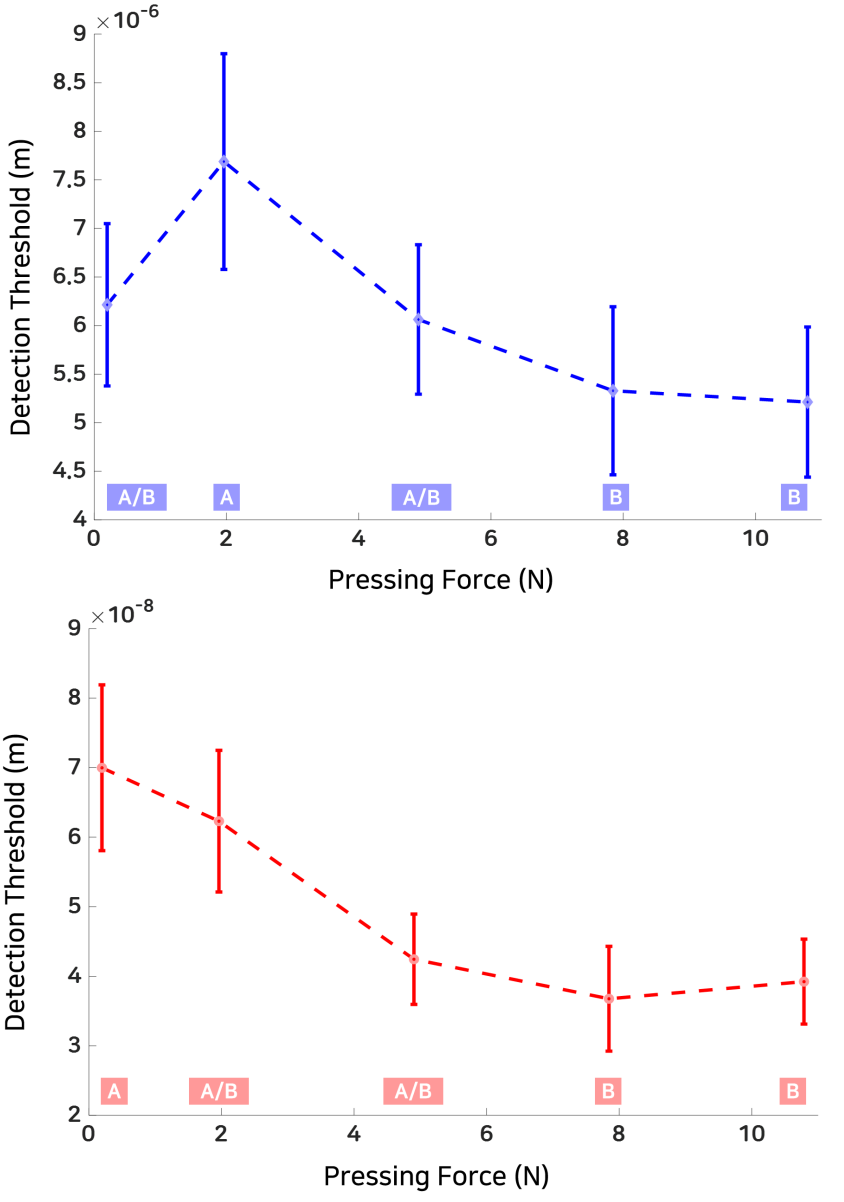

Figure 5.3: Absolute thresholds in terms of peak displacement measured for each ***Freq*** condition. Error bars show standard errors. For each frequency, data points marked with different letters were different with statistical significance.

differences at each ***Press*** level were 39.33, 42.54, 43.26, 43.82, and 42.79 dB, respectively.

Second, out of the two ***Freq*** levels, we performed one-way repeated measures ANOVA for ***Press*** on the 40 Hz conditions only (Figure 5.3, top). The detection thresholds were significantly affected by changes in ***Press*** ($F(4, 36) = 3.27, p = 0.022$). For post-hoc analysis, we used Tukey's honest significant difference test. The results showed that the 2.0 N condition produced a significantly higher threshold than the 7.8 and 10.8 N conditions (Figure 5.3,top). No other significant differences in threshold were observed. Therefore, for 40 Hz vibration, we can say that the absolute threshold increased to pressing force between 2.0 and 4.9 N, and it began to decrease thereafter. We will revisit this interesting result in Section 5.4.

Third, one-way repeated measures ANOVA for ***Press*** on the 250 Hz data suggested that the detection thresholds were significantly affected ($F(4, 36) = 4.55, p = 0.0045$) by the exerted active force (Figure 5.3, bottom). Subsequent Tukey's test revealed that the vibrotactile sensitivities for the 7.8 and 10.8 N conditions were significantly better than the lowest sensitivity value at the 0.2 N condition (Figure 5.3,bottom). There were no significant differences among the other four higher-sensitivity ***Press*** levels (2.0, 4.9, 7.8, and 10.8 N). These results indicate that the absolute threshold decreased until ***Press*** was 7.8 N, and the absolute thresholds did not decrease once the pressing force exceeded 7.8 N.

Table 5.1: Means and Standard Deviations of Force Control Error (***CtrlErr***), and the Means of Accuracy and Precision

Press (N)	***CtrlError*** (N)	**Accuracy** (%)	**Precision** (%)
	mean ± s.d.	mean	mean
0.2	0.033 ± 0.027	16.73	11.71
2.0	-0.031 ± 0.091	-1.57	4.72
4.9	-0.131 ± 0.161	-2.68	3.38
7.8	-0.396 ± 0.304	-5.04	4.08
10.8	-0.633 ± 0.456	-5.87	4.49

5.3.2 Pressing Force

We recorded the participants' pressing forces in all trials and intervals (with/without vibration) to verify their ability to control pressing force. The control error of pressing force (***CtrlErr***) was calculated by subtracting the target pressing force from the measured pressing force, which represents the accuracy of force control. The means and standard deviations of ***CtrlErr*** are provided in Table 5.1. A three-way repeated measures ANOVA was performed to test the effect of ***Press***, ***Freq***, and the presence of vibrotactile stimulus on ***CtrlErr***. Only ***Press*** was found to be a significant factor ($F(4, 36) = 22.45, p<.0001$; Figure 5.4). Vibration frequency ($F(1, 9) = 0.016, p = 0.901$) or the existence of stimulus ($F(1, 9) = 0.05, p = 0.829$) did not affect the participants' force control, nor did any of the interaction terms.

The absolute value of ***CtrlErr*** generally increased as ***Press*** increased. The error was negative in all the conditions except when the target pressing force

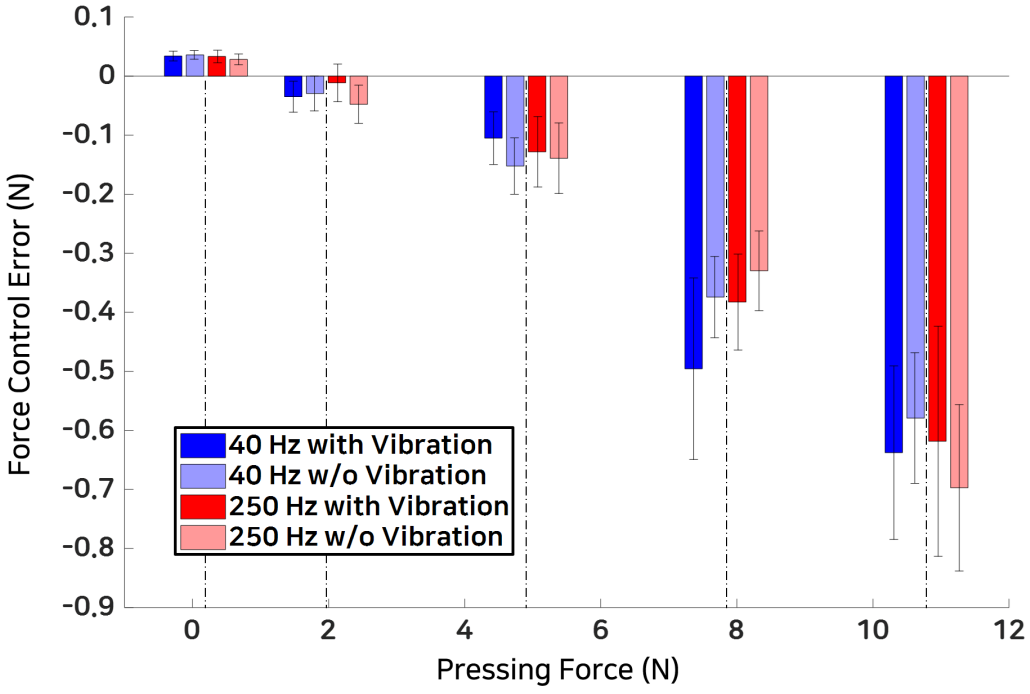

Figure 5.4: Mean force control errors with standard errors (error bars) for each frequency and the existence/absence of vibrotactile stimulus.

was 0.2 N (Figure 5.4), exhibiting overshoots. The mean values of ***CtrlErr*** were larger than 0.29 N at the two highest pressing forces (7.8 and 10.8 N) because there were some instances where participants had difficulties in maintaining the two pressing forces. The means of ***CtrlErr*** were normalized by the target forces, and these values are shown in Table 5.1. The normalized accuracy was not good (16.73%) for the lowest pressing force (0.2 N for mere contact), but it stayed within 5.87% with undershoots for the other target forces. As a measure of precision, we inspected the standard deviations of ***CtrlErr*** normalized by the means of the measured pressing forces. These precision values are also shown in the last

column of Table 5.1. It was 11.71% for the lowest pressing force but ranged from 3.38% to 4.72% for the other larger target forces. All these results suggest that the participants could control the pressing force accurately and precisely unless the target force was very low, corresponding to merely maintaining contact.

5.4 Discussion

We have reported psychophysical measurements that represent vibrotactile sensitivity when both stimulus frequency and active pressing force are varied. Our absolute threshold curves indicate the intensities of vibrotactile stimuli that lead to 70.7% correct detection. Two absolute threshold curves for 40 and 250 Hz stimuli, innervating the different information processing channels (RA-I and PC channel, respectively), were derived from our measurements. In this section, we discuss the experimental results in detail, often in comparison with the relevant knowledge available in the literature.

The absolute threshold plots shown in Figure 5.2 manifest the effects of vibration frequency and pressing force. A distinctive finding was that the absolute thresholds increased and later decreased as the pressing force increased when the frequency was 40 Hz, while they generally decreased for 250 Hz.

5.4.1 Effects of Vibration Frequency

The experimental results demonstrate intriguing contrast between the behavior of the two rapidly-adapting mechanoreceptive channels as to the effect of pressure. Such perceptual data are rare in the literature. In [50], where 250 Hz sinusoidal vibration was used with active pressing forces of 1.9, 8, and 15 N (contact

site: finger pad; unregulated contact area), absolute thresholds clearly decreased with the increasing pressing forces. This trend was also apparent in our study, where absolute thresholds for 250 Hz vibration were measured for the five pressing forces ranging from 0.2 to 10.8 N under the controlled contact area. These results, since 250 Hz vibration is dominantly mediated by the PC channel at the threshold level [45], imply that stronger active pressure increases the vibrotactile sensitivity of the PC channel.

Interestingly, our absolute thresholds for 40 Hz vibration exhibited the different pattern: the increasing trend in the thresholds presented a transition to decreasing with further pressing force increase. In [100, Figure 10], absolute thresholds measured with one participant are shown as a function of frequency for four *static* contact forces (0.1, 0.5, 1.5, and 4.5 N), where contact force was passively maintained by externally controlling the indentation depth of the contactor to the skin. The contactor was placed on the arm without a surround. When the vibration frequency was very low (below 20 Hz), the absolute thresholds clearly increased as the static contact force increased. It appears that the RA-I channel has diminished vibrotactile sensitivity when the skin is subject to increased contact pressure. In [100, Figure 10], however, the opposite (decreasing) pattern was found for the vibration frequencies above 50 Hz, similar to our 250 Hz thresholds. Between 20 Hz and 50 Hz, the threshold data showed a transition from increasing to decreasing as the static force increased. This pattern is what we observed with our 40 Hz thresholds with *active* pressing force. Therefore, according to our absolute thresholds for 40 Hz vibration (ten participants;

contact site: finger pad; 1.45 cm^2 without surround) and those for the frequencies around 40 Hz in [100, Figure 10] (single participant; contact site: inner side of forearm; contactor: 1.5 cm^2 without surround), something causes a sensitivity crossover for 40 Hz vibration with respect to increasing contact pressure.

5.4.2 Effects of Pressing Force

The biomechanical structure of sensory organs can be deformed when they are exposed to external contact force. Meissner and Pacinian corpuscles, which are the end organs of the RA-I and PC channels, respectively, have different mechanical structures, and their sensitivity depends on the surrounding receptor structure as well as the transducing nerve endings [111]. Meissner corpuscles are relatively large, and they reside in the dermal ridges lying just beneath the epidermis. They have cell layers that enclose the large endings of two to six RA-I afferent fibers, and this pillow-like structure functions as a filter that prevents static skin deformation from affecting the velocity-sensitive endings [111]. Thus, when large external pressure deforms the skin, the surrounding layers of Meissner corpuscles under the influence are likely to become distorted (personal communication with Sung Jun Jung). In such a loaded situation, stronger vibration may be necessary to trigger the nerve endings of Meissner corpuscles. In contrast, Pacinian corpuscles are in the deep dermis, and they are much less likely to be affected by external pressure.

Transmission of a vibratory stimulus into the skin is also largely affected by the biomechanical properties of the hand and its skin [69]. Mann and Griffin investigated the effect of contact force (0.25 to 8 N) on the mechanical impedance

of the distal phalanx of the index finger [31]. Greater contact force generally encountered higher mechanical impedance [31, Figure 5]. The impedance differences for contact force ranging from 1 to 8 N were more evident at 40 Hz than at 250 Hz. Increased mechanical impedance implies that a stronger vibrotactile stimulus is required to achieve the same indentation on the skin. This may also be responsible for the increased detection thresholds at the low contact force levels (0.2 and 2.0 N) for the 40 Hz condition in our study. Furthermore, when the skin tissues are compressed, the transmissibility of vibration is higher at 250 Hz vibration, e.g., from the hand to the wrist [112] and from the fingertip to the distal, middle, and proximal phalanxes [30], by coupling vibrations transmitted to bones and tendons (personal communication with Sung Jun Jung; also see [49]). This may account for the decreased thresholds for 250 Hz vibration as pressing force increased.

Going back to our results from the 40 Hz conditions (Figure 5.3, top), the initially declining vibrotactile sensitivity started to increase for contact force somewhere between 2.0 to 4.9 N. We suspect that this stems from a crossover of the dominant information processing channel from RA-I to PC, between the two rapidly-adapting channels. When the contactor area was 145 mm^2, the RA-I channel had a lower absolute threshold for 40 Hz vibration than the PC channel when no external pressure is applied (see [113, Figure 7]). Increasing contact pressure degrades the sensitivity of the RA-I channel to 40 Hz vibration while it improves the sensitivity of the PC channel, eventually leading to the observed crossover. A similar example was previously reported in the forearm [100, Figure

10].

5.4.3 Comparisons of Absolute Thresholds

The absolute thresholds reported in this article can be compared to those published earlier in the literature. For example, Papetti et al. [50] presented absolute thresholds for 250 Hz vibration under active pressing forces. These thresholds were considerably lower than our measurements (compare Fig. 5.2 and [50, Table 1]). The differences in the thresholds could have been due to the temporal energy integration property of the PC channel. In [50], A longer stimulus duration (1.5 s) than our experimental condition (1 s) was used in the experiment. The fact that the contactor was a flat surface in [50] could also have contributed to the threshold differences.

Finally, a comparison of our absolute threshold measurements with those found in other prior studies is summarized in Table 5.2. The previous studies listed in the table were concerned with vibrotactile sensitivity on the fingertip. All thresholds were converted to have a unit of decibels relative to 1 μm (peak). Our threshold results at the two lowest force levels (0.2 and 2.0 N; 1.45 cm^2 contactor area) were similar to those of Lamoré and Keemink (0.5 N $\pm$0.2 N; 1.5 cm^2) [100], Goble et al. (assumed to be 0.3 N; 1.4 cm^2 effective contact area) [99], Verrillo (not specified; 0.005 cm^2 for 40 Hz and 1.3 cm^2 for 250 Hz) [114], and Harada and Griffin (2 N; 0.385 cm^2) [106]. Our thresholds were not very different from those found by the others, and the differences did not exceed 5.3 dB.

Table 5.2: Comparison of Detection Thresholds in Peak Displacement Amplitude of Sinusoidal Vibrations Transmitted to the Fingertip for Two Frequencies and Two Pressing Forces (units are in dB re 1 μm; † denotes interpolated values; underline for static force cases and **bold** for active force cases).

$\sim$ 0.2 N								
Frequency (Hz)	**25**		**40**	**50**		**214.4**	**250**	**375.2**
Lamoré and Keemink in Fig. 2 [100]	-	-	12.58	-	-	-26.18	-26.05†	-25.60
Goble et al. [99]	17.56	-	9.97 †	4.91	-	-	-25.97	-
Verrillo [114]	-	-	12.05	-	-	-	-21.82	-
Present study	-	-	**15.25**	-	-	-	**-24.08**	-
$\sim$ 2.0 N								
Frequency (Hz)		**31.6**	**40**		**60**		**250**	
Harada and Griffin [106]	-	24.03	18.50 †	-	3.35	-	-21.57	-
Papetti et al. [50]	-	-	-	-	-	-	**-48.7**	-
Present study	-	-	**16.94**	-	-	-	**-25.60**	-

5.5 Conclusions

In this chapter, we explored how the perceptual characteristics of vibrotactile stimuli is affected by two experimental variables, active pressing force and vibration frequency, concentrating on the sensitivity. We measured the absolute thresholds for two sinusoidal vibrations (40 and 250 Hz) under five pressing forces (0.2, 2.0, 4.9, 7.8, and 10.8 N). The results showed distinctive tendencies in the sensitivity over the pressing forces at the two levels of frequency. The main findings of our experiment were as follows: 1) the sensitivity to 250 Hz stimuli generally increased with increasing pressing force; 2) the sensitivity to 40 Hz stimuli initially decreased but then increased after the contact force exceeded 2 N; and 3) the participants were more sensitive to 250 Hz stimuli than 40 Hz stimuli by at least 39.33 dB (at 0.2 N), and the sensitivity gap between the two frequencies generally increased as the pressing force increased. In future studies, we will investigate the effectiveness of vibrotactile rendering based on the results of this study and explore the design space of vibrotactile feedback and force-sensitive input.

VI. Conclusion

6.1 Contributions

In this thesis, the main contributions are summarized as follows:

- Investigate vibration transmissibility in various contexts, e.g., the hand, rigid surfaces, everyday objects, and various material, and explore its applications in Human-Computer Interaction.
- Verify the possibility of vibration as a sensing channel for input interaction in tangible interaction
- Unveil the perception of vibrotactile stimuli during active haptic interaction

There are primarily two major topics pertinent to this dissertation: vibration-based sensing technique and vibrotactile feedback. The former stresses the usage of vibration as a sensing channel. Compared to other sensing channels, vibration has the unique characteristic of being a mechanical wave which tells us about the physical properties of a medium, e.g., weight, elasticity, and damping, during its propagation. By leveraging such a characteristic, I have been working on how to imbue computing capability into plain everyday objects. The propagation of vibration has been fully investigated in the relevant context when a user touches a surface or object. This investigation is the foundation of the first attempt to augment the hand with vibration.

When it comes to vibrotactile feedback, the primary achievement is to fully characterize the sensory channel in the context of use. When utilizing physical props for the execution of fine manual tasks, we need to precisely control the force applied to the props. In order to deliver reliable tactile feedback during such dexterous manual tasks, the author conducted a psychophysical experiment for understanding the fundamentals in vibrotactile perception. On top of this fundamental understanding of human vibrotactile perception, I have explored a number of ways to advance vibrotactile rendering with collaborators, such as adding impulsive force to improve the realism of tactile sensation, optimizing illusory moving tactile sensation, and designing illusory penetrating tactile sensation.

6.2 Future Directions

The primary reason for which I would like to engage in HCI research is the versatility offered. For myself, the design process of interactive artifacts is like instilling life to them. As such, the research topics in this dissertation and other co-works cover broad topics in HCI, such as human perception, sensing, and feedback. I envision converging the findings from these previous works to shed light on the next level of haptic interaction.

Previously, sensing and actuation have been two distinct research topics in many cases. In future work, I would like to design systematic haptic feedback bridging detected actions and desired motions. When the input and output of a system are modeled together, it is possible to seamlessly present information that

helps adjust the sensory-motor coordination. Simultaneous and continuous sensory feedback, e.g., beep intervals while driving backward to notify the distance to walls, assist us in performing fine motor tasks. I have an interest in exploring tactile feedback which inhibits or induces desired motor actions, enhancing usability, e.g., the spatial control of AR user interfaces, and user experience, e.g., haptic signifier and feedforward.

Secondly, the dimension of vibrotactile feedback can be extended toward a volume or surface. Previously, vibration has delivered to the skin as a single point stimulus, e.g., to the fingertip, although surface haptic devices have received research attention. The purpose of this future work is to intentionally localize vibration over a surface or across a volume so as to generate a pattern which can be simultaneously perceived by a wide area of the user's skin. My idea concerns the computational design of specially structured patterns or materials to intentionally control the transmission of vibration. In other words, the propagation of vibration can be further compounded by metamaterials or non-newtonian fluid blocking and transmitting vibration across a surface or a volume.

요 약 문

우리는 일상에서 다양한 물건을 사용하고 조작하는 과정을 통해서 필요한 과업을 수행하게 된다. 이러한 실물 객체와의 상호작용 경험은 오랜 시간에 걸쳐 누적되고 체화된다. 본 연구에서는 인간에게 체화된 촉각적 상호작용 경험을 가상의 컴퓨팅 환경으로 확장하기 위한 일련의 연구를 진행하였다. 이를 인간 컴퓨터 상호작용의 입출력 관점으로 나누어서 각각을 살펴보면 다음과 같다.

첫 번째 단계로 사용자가 일상적인 물체를 유형의 입력 장치로 사용할 수 있도록, 진동을 사용자의 입력 인식을 위한 매체로 사용하는 가능성에 대해서 살펴보았다. 사용자가 손을 사용하여 텐저블 인터페이스와 상호작용을 시작하기 위해서는 필연적으로 물체와 접촉하게 된다. 이때, 사용자가 물체와 접촉하는 접촉 상태와 사용자가 접촉한 물체 자체를 인식하는 두 가지의 인식 기술에 대해서 탐구하였다.

첫 번째 인식 기술은 사용자가 강체 표면과 접촉하는 순간, 사용자의 손가락에 위치한 진동 링에서 특정 주파수가 인코딩된 진동 신호를 내보내고, 이를 강체 표면에 부착된 마이크로 인식하는 과정을 거친다. 일련의 신호 처리 및 기계 학습 모델의 계산 과정을 통해서, 강체 표면과 접촉한 손가락을 찾아내는 연구를 수행하였다.

두 번째 인식 기술은 사용자가 손에 쥐고 있는 물체를 인식하는 기술이다. 사용자의 한쪽 손가락에서 발생시킨 진동이 물체를 투과하여 반대편 손가락의 가속도계에서 해당 진동 신호를 수집한다. 이때, 수집된 진동 가속도 신호는 기계적 임피던스 특성에 따라서 물체를 구성하고 있는 물질의 차이에 따라 서로 다르게 왜곡된 형태를 띤다. 이러한 현상을 이용하여, 물체별로 다르게 왜곡된 가속도 신호의 패턴을

분류기가 학습하고 높은 정확도로 분류하는 연구를 수행하였다.

두 번째 단계로 사용자가 이러한 유형의 입력 장치를 통해서 컴퓨팅 환경과 상호작용할 때, 사용자가 수행하는 수동 작업의 복잡도가 높아질수록 미세한 힘의 조절은 필수적이다. 사용자와 텐저블 인터페이스 간의 상호작용을 효과적으로 매개하기 위하여, 사용자가 능동적으로 표면을 누르는 상황에서 진동에 대한 사용자의 촉각적 인지 실험을 수행하였다. 본 연구에서는 사용자가 수동 작업 중에 사용하는 넓은 영역의 압력 범위와 두 개의 특징적인 진동 주파수에 따라서 진동 민감도를 측정하였다. 사용된 두 개의 주파수에 따라서 가해진 압력에 따른 진동 민감도의 경향성이 상이한 것을 확인할 수 있었다.

References

[1] Ivan Poupyrev, Mark Billinghurst, Suzanne Weghorst, and Tadao Ichikawa. The go-go interaction technique. In *Proceedings of the 9th annual ACM symposium on User interface software and technology - UIST '96*, pages 79–80, New York, New York, USA, 1996. ACM Press.

[2] Edwin L. Hutchins, James D. Hollan, and Donald A. Norman. Direct Manipulation Interfaces. *Human-Computer Interaction*, 1(4):311–338, dec 1985.

[3] Doug A. Bowman, Ryan P. McMahan, and Eric D. Ragan. Questioning naturalism in 3D user interfaces. *Communications of the ACM*, 55(9):78, sep 2012.

[4] Ben. Shneiderman. *Designing the user interface : strategies for effective human-computer-interaction.* 2010.

[5] Hiroshi Ishii. Tangible bits: Beyond pixels. *TEI'08 - Second International Conference on Tangible and Embedded Interaction - Conference Proceedings*, 2008.

[6] Paul Dourish. *Where the action is: the foundations of embodied interaction.* MIT press, 2004.

[7] Jungchan Cho, Inhwan Hwang, and Songhwai Oh. VibePhone: efficient surface recognition for smartphones using vibration. *Pattern Analysis and Applications*, 19(1):251–265, feb 2016.

[8] Xing-Dong Yang, Tovi Grossman, Daniel Wigdor, and George Fitzmaurice. Magic finger: Always-available input through finger instrumentation. In *Proceedings of the 25th Annual ACM Symposium on User Interface Software and Technology*, UIST '12, pages 147–156, New York, NY, USA, 2012. ACM.

[9] Hui-Shyong Yeo, Gergely Flamich, Patrick Schrempf, David Harris-Birtill, and Aaron Quigley. Radarcat: Radar categorization for input & interaction. In *Proceedings of the 29th Annual Symposium on User Interface Software and Technology*, UIST '16, pages 833–841, New York, NY, USA, 2016. ACM.

[10] Gierad Laput, Robert Xiao, and Chris Harrison. Viband: High-fidelity bio-acoustic sensing using commodity smartwatch accelerometers. In *Proceedings of the 29th Annual Symposium on User Interface Software and Technology*, UIST '16, pages 321–333, New York, NY, USA, 2016. ACM.

[11] Chris Harrison and Scott E. Hudson. Lightweight material detection for placement-aware mobile computing. In *Proceedings of the 21st Annual ACM Symposium on User Interface Software and Technology*, UIST '08, pages 279–282, New York, NY, USA, 2008. ACM.

[12] Youngjun Cho, Nadia Bianchi-Berthouze, Nicolai Marquardt, and Simon J. Julier. Deep thermal imaging: Proximate material type recognition in the wild through deep learning of spatial surface temperature patterns. In *Proceedings of the 2018 CHI Conference on Human Factors in Computing Systems*, CHI '18, pages 2:1–2:13, New York, NY, USA, 2018. ACM.

[13] Seungmoon Choi and Katherine J. Kuchenbecker. Vibrotactile display: Perception, technology, and applications. *Proceedings of the IEEE*, 101(9):2093–2104, 2013.

[14] Enrico Concettoni and Michael J. Griffin. The apparent mass and mechanical impedance of the hand and the transmission of vibration to the fingers, hand, and arm. *Journal of Sound and Vibration*, 325(3):664–678, 2009.

[15] A Amin, Damione Wright, and Ian Howard. The measurement of vibration transmissibility and mechanical impedance of resilient materials as a function of coverage area to improve anti-vibration glove design. In *PROCEEDINGS OF ISMA2016 INTERNATIONAL CONFERENCE ON NOISE AND VIBRATION ENGINEERING AND USD2016 INTERNATIONAL CONFERENCE ON UNCERTAINTY IN STRUCTURAL DYNAMICS*, pages 1105–1116, 2016.

[16] Timothy G Gutowski and Clive L Dym. Propagation of ground vibration: a review. *Journal of Sound and Vibration*, 49(2):179–193, 1976.

[17] G. Park, H. Cha, and S. Choi. Haptic enchanters: Attachable and detachable vibrotactile modules and their advantages. *IEEE Transactions on Haptics*, 12(1):43–55, Jan 2019.

[18] Gi-Hun Yang, Moon-sub Jin, Yeonsub Jin, and Sungchul Kang. T-mobile: Vibrotactile display pad with spatial and directional information for handheld device. In *2010 IEEE/RSJ International Conference on Intelligent Robots and Systems*, pages 5245–5250, Oct 2010.

[19] D. Ryu, G. Yang, and S. Kang. T-hive : Vibrotactile interface presenting spatial information on handle surface. In *2009 IEEE International Conference on Robotics and Automation*, pages 683–688, May 2009.

[20] Koji Yatani and Khai Nhut Truong. Semfeel: A user interface with semantic tactile feedback for mobile touch-screen devices. In *Proceedings of the 22Nd Annual ACM Symposium on User Interface Software and Technology*, UIST '09, pages 111–120, New York, NY, USA, 2009. ACM.

[21] Hugo Nicolau, Kyle Montague, Tiago Guerreiro, André Rodrigues, and Vicki L. Hanson. Holibraille: Multipoint vibrotactile feedback on mobile devices. In *Proceedings of the 12th Web for All Conference*, W4A '15, pages 30:1–30:4, New York, NY, USA, 2015. ACM.

[22] Marco Fabiani. Development of a tangible human-machine interface exploiting in-solid vibrational signals acquired by multiple sensors. *KTH Stockholm*, 58, 2006.

[23] Yiran Zhao, Shuochao Yao, Shen Li, Shaohan Hu, Huajie Shao, and Tarek F. Abdelzaher. Vibebin: A vibration-based waste bin level detection system. volume 1, pages 122:1–122:22, New York, NY, USA, September 2017. ACM.

[24] Makoto Ono, Buntarou Shizuki, and Jiro Tanaka. Touch & activate: Adding interactivity to existing objects using active acoustic sensing. In *Proceedings of the 26th Annual ACM Symposium on User Interface Software and Technology*, UIST '13, pages 31–40, New York, NY, USA, 2013. ACM.

[25] Makoto Ono, Buntarou Shizuki, and Jiro Tanaka. Sensing touch force using active acoustic sensing. In *Proceedings of the Ninth International Conference on Tangible, Embedded, and Embodied Interaction*, TEI '15, pages 355–358, New York, NY, USA, 2015. ACM.

[26] Jian Liu, Chen Wang, Yingying Chen, and Nitesh Saxena. VibWrite. pages 73–87, 2017.

[27] Tauhidur Rahman, Alexander Travis Adams, Mi Zhang, Erin Cherry, Bobby Zhou, Huaishu Peng, and Tanzeem Choudhury. Bodybeat: a mobile system for sensing non-speech body sounds. In *MobiSys*, volume 14, pages 2–13. Citeseer, 2014.

[28] Katherine O. Sofia and Lynette Jones. Mechanical and psychophysical studies of surface wave propagation during vibrotactile stimulation. *IEEE Transactions on Haptics*, 6(3):320–329, 2013.

[29] Bharat Dandu, Yitian Shao, Andrew Stanley, and Yon Visell. Spatiotemporal Haptic Effects from a Single Actuator via Spectral Control of Cutaneous Wave Propagation. (July):425–430, 2019.

[30] H. Schafer, Z. Wells, Y. Shao, and Y. Visell. Transfer properties of touch elicited waves: Effect of posture and contact conditions. In *2017 IEEE World Haptics Conference (WHC)*, pages 546–551, June 2017.

[31] N A Mann and M J Griffin. Effect of contact conditions on the mechanical impedance of the finger. *Central European journal of public health*, 4(1):46–9, feb 1996.

[32] Chris Harrison, Desney Tan, and Dan Morris. Skinput: Appropriating the Body as an Input Surface. In *Proceedings of the 28th international conference on Human factors in computing systems - CHI '10*, volume 3, page 453, 2010.

[33] Maotian Zhang, Qian Dai, Panlong Yang, Jie Xiong, Chang Tian, and Chaocan Xiang. iDial. *Proceedings of the ACM on Interactive, Mobile, Wearable and Ubiquitous Technologies*, 2(1):1–20, 2018.

[34] Yongzhi Huang, Shaotian Cai, Lu Wang, and Kaishun Wu. Oinput: A Bone-Conductive QWERTY Keyboard Recognition for Wearable Device. *Proceedings of the International Conference on Parallel and Distributed Systems - ICPADS*, 2018-Decem:946–953, 2019.

[35] Wenqiang Chen, Maoning Guan, Yandao Huang, Lu Wang, Rukhsana Ruby, Wen Hu, and Kaishun Wu. ViType: A cost efficient on-body typing

system through vibration. *2018 15th Annual IEEE International Conference on Sensing, Communication, and Networking, SECON 2018*, pages 1–9, 2018.

[36] Yu-Chih Tung and Kang G. Shin. Expansion of human-phone interface by sensing structure-borne sound propagation. In *Proceedings of the 14th Annual International Conference on Mobile Systems, Applications, and Services*, MobiSys '16, pages 277–289, New York, NY, USA, 2016. ACM.

[37] Jian Liu, Yingying Chen, Marco Gruteser, and Yan Wang. VibSense: Sensing Touches on Ubiquitous Surfaces through Vibration. In *2017 14th Annual IEEE International Conference on Sensing, Communication, and Networking, SECON 2017*, pages 1–9. IEEE, 2017.

[38] Nobuhiro Funato and Kentaro Takemura. Grip force estimation by emitting vibration. In *Adjunct Publication of the 30th Annual ACM Symposium on User Interface Software and Technology*, UIST 17, pages 141–142, New York, NY, USA, 2017. Association for Computing Machinery.

[39] Yuya Okawa and Kentaro Takemura. Haptic-enabled Active Bone-Conducted Sound Sensing. *Proceedings of the 28th Annual ACM Symposium on User Interface Software & Technology - UIST '15 Adjunct*, pages 87–88, 2015.

[40] Hiroyuki Kato and Kentaro Takemura. Hand pose estimation based on active bone-conducted sound sensing. In *Proceedings of the 2016 ACM*

International Joint Conference on Pervasive and Ubiquitous Computing: Adjunct, UbiComp '16, pages 109–112, New York, NY, USA, 2016. ACM.

[41] Cheng Zhang, Qiuyue Xue, Anandghan Waghmare, Ruichen Meng, Sumeet Jain, Yizeng Han, Xinyu Li, Kenneth Cunefare, Thomas Ploetz, Thad Starner, Omer Inan, and Gregory D. Abowd. Fingerping: Recognizing fine-grained hand poses using active acoustic on-body sensing. In *Proceedings of the 2018 CHI Conference on Human Factors in Computing Systems*, CHI '18, pages 437:1–437:10, New York, NY, USA, 2018. ACM.

[42] Wei Wang, Lin Yang, and Qian Zhang. Resonance-based Secure Pairing for Wearables. *IEEE Transactions on Mobile Computing*, 1233(c):1–1, 2018.

[43] Yang Zhang, Gierad Laput, and Chris Harrison. Vibrosight: Long-range vibrometry for smart environment sensing. In *Proceedings of the 31st Annual ACM Symposium on User Interface Software and Technology*, UIST '18, pages 225–236, New York, NY, USA, 2018. ACM.

[44] Kai Kunze and Paul Lukowicz. Symbolic object localization through active sampling of acceleration and sound signatures. In *Proceedings of the 9th International Conference on Ubiquitous Computing*, UbiComp '07, pages 163–180, Berlin, Heidelberg, 2007. Springer-Verlag.

[45] George A. Gescheider, John H. Wright, and Ronald T. Verrillo. *Information-processing channels in the tactile sensory system: A psychophysical and physiological analysis.* Psychology Press, 2008.

[46] Lynette A Jones and Susan J Lederman. *Human Hand Function*, volume 32. 2006.

[47] Heather Culbertson, Samuel B Schorr, and Allison M Okamura. Haptics: The present and future of artificial touch sensation. *Annual Review of Control, Robotics, and Autonomous Systems*, 1:385–409, 2018.

[48] Stanley J. Bolanowski, George A. Gescheider, and Ronald T. Verrillo. Hairy skin: Psychophysical channels and their physiological substrates. *Somatosensory & Motor Research*, 11(3):279–290, 1994.

[49] A. J. Brisben, S. S. Hsiao, and K. O. Johnson. Detection of Vibration Transmitted Through an Object Grasped in the Hand. *J Neurophysiol*, 81(4):1548–1558, 1999.

[50] Stefano Papetti, Hanna Järveläinen, Bruno L. Giordano, Sébastien Schiesser, and Martin Fröhlich. Vibrotactile sensitivity in active touch: Effect of pressing force. *IEEE Transactions on Haptics*, 10(1):113–122, 2017.

[51] Huy Viet Le, Sven Mayer, and Niels Henze. Infinitouch: Finger-aware interaction on fully touch sensitive smartphones. In *Proceedings of the 31st Annual ACM Symposium on User Interface Software and Technology*, UIST 18, pages 779–792, New York, NY, USA, 2018. Association for Computing Machinery.

[52] Srinath Sridhar, Anders Markussen, Antti Oulasvirta, Christian Theobalt, and Sebastian Boring. Watchsense: On- and above-skin input sensing

through a wearable depth sensor. In *Proceedings of the 2017 CHI Conference on Human Factors in Computing Systems*, CHI 17, pages 3891–3902, New York, NY, USA, 2017. Association for Computing Machinery.

[53] Hyunjae Gil, DoYoung Lee, Seunggyu Im, and Ian Oakley. Tritap: Identifying finger touches on smartwatches. In *Proceedings of the 2017 CHI Conference on Human Factors in Computing Systems*, CHI 17, pages 3879–3890, New York, NY, USA, 2017. Association for Computing Machinery.

[54] Huy Viet Le, Sven Mayer, and Niels Henze. Investigating the feasibility of finger identification on capacitive touchscreens using deep learning. In *Proceedings of the 24th International Conference on Intelligent User Interfaces*, IUI 19, pages 637–649, New York, NY, USA, 2019. Association for Computing Machinery.

[55] Keunwoo Park and Geehyuk Lee. Fingmag: Finger identification method for smartwatch. In *Extended Abstracts of the 2019 CHI Conference on Human Factors in Computing Systems*, CHI EA 19, New York, NY, USA, 2019. Association for Computing Machinery.

[56] Christian Holz and Patrick Baudisch. Fiberio: A touchscreen that senses fingerprints. In *Proceedings of the 26th Annual ACM Symposium on User Interface Software and Technology*, UIST 13, pages 41–50, New York, NY, USA, 2013. Association for Computing Machinery.

[57] Vincent Becker, Pietro Oldrati, Liliana Barrios, and Gábor Sörös. Touchsense: Classifying finger touches and measuring their force with an elec-

tromyography armband. In *Proceedings of the 2018 ACM International Symposium on Wearable Computers*, ISWC 18, pages 1–8, New York, NY, USA, 2018. Association for Computing Machinery.

[58] Hrvoje Benko, T. Scott Saponas, Dan Morris, and Desney Tan. Enhancing input on and above the interactive surface with muscle sensing. In *Proceedings of the ACM International Conference on Interactive Tabletops and Surfaces*, ITS 09, pages 93–100, New York, NY, USA, 2009. Association for Computing Machinery.

[59] Nicolai Marquardt, Johannes Kiemer, David Ledo, Sebastian Boring, and Saul Greenberg. Designing user-, hand-, and handpart-aware tabletop interactions with the touchid toolkit. In *Proceedings of the ACM International Conference on Interactive Tabletops and Surfaces*, ITS 11, pages 21–30, New York, NY, USA, 2011. Association for Computing Machinery.

[60] Alix Goguey, Géry Casiez, Daniel Vogel, Fanny Chevalier, Thomas Pietrzak, and Nicolas Roussel. A three-step interaction pattern for improving discoverability in finger identification techniques. In *Proceedings of the Adjunct Publication of the 27th Annual ACM Symposium on User Interface Software and Technology*, UIST14 Adjunct, pages 33–34, New York, NY, USA, 2014. Association for Computing Machinery.

[61] Andrea Bianchi and Seungwoo Je. Disambiguating touch with a smart-ring. In *Proceedings of the 8th Augmented Human International Conference*, AH 17, New York, NY, USA, 2017. Association for Computing Machinery.

[62] Chih-Pin Hsiao, Richard Li, Xinyan Yan, and Ellen Yi-Luen Do. Tactile teacher: Sensing finger tapping in piano playing. In *Proceedings of the Ninth International Conference on Tangible, Embedded, and Embodied Interaction*, TEI 15, pages 257–260, New York, NY, USA, 2015. Association for Computing Machinery.

[63] Damien Masson, Alix Goguey, Sylvain Malacria, and Géry Casiez. Whichfingers: Identifying fingers on touch surfaces and keyboards using vibration sensors. In *Proceedings of the 30th Annual ACM Symposium on User Interface Software and Technology*, UIST 17, pages 41–48, New York, NY, USA, 2017. Association for Computing Machinery.

[64] Aakar Gupta and Ravin Balakrishnan. Dualkey: Miniature screen text entry via finger identification. In *Proceedings of the 2016 CHI Conference on Human Factors in Computing Systems*, CHI 16, pages 59–70, New York, NY, USA, 2016. Association for Computing Machinery.

[65] Aakar Gupta, Muhammed Anwar, and Ravin Balakrishnan. Porous interfaces for small screen multitasking using finger identification. In *Proceedings of the 29th Annual Symposium on User Interface Software and Technology*, UIST 16, pages 145–156, New York, NY, USA, 2016. Association for Computing Machinery.

[66] Namhyun Kim, Junseong Lee, Joyce Jiyoung Whang, and Jinkyu Lee. SmartGrip: grip sensing system for commodity mobile devices through sound signals. *Personal and Ubiquitous Computing*, 2019.

[67] Angelo Farina. Advancements in impulse response measurements by sine sweeps. *Audio Engineering Society - 122nd Audio Engineering Society Convention 2007*, 3(September 2004):1626–1646, 2007.

[68] Stratasys. Tango, 2019. Retrieved December 7, 2019 from `https://www.stratasys.com/materials/search/tango`.

[69] Inwook Hwang, Jongman Seo, Myongchan Kim, and Seungmoon Choi. Vibrotactile perceived intensity for mobile devices as a function of direction, amplitude, and frequency. *IEEE Transactions on Haptics*, 2013.

[70] Sebastian Merchel, Mehmet Ercan Altinsoy, Sebastian Merchel, Mehmet Ercan, and Altinsoy Psychophysical. Psychophysical Comparison of the Auditory and Vibrotactile Perception-Absolute Sensitivity To cite this version : HAL Id : hal-02007390 Psychophysical Comparison of the Auditory and Vibrotactile Perception - Absolute Sensitivity. 2019.

[71] ISO. ISO 226:2003 - Acoustics – Normal equal-loudness-level contours, 08 2003. Retrieved December 7, 2019 from `https://www.iso.org/standard/34222.html`.

[72] Alain Dufaux. Detection and Recognition of Impulsive Sound Signals. *Institute de Microtechnique Neuchatel, Switzerland*, (January), 2001.

[73] Lei Shi, Maryam Ashoori, Yunfeng Zhang, and Shiri Azenkot. Knock knock, What's there: Converting passive objects into customizable smart controllers. *MobileHCI 2018 - Beyond Mobile: The Next 20 Years - 20th*

International Conference on Human-Computer Interaction with Mobile Devices and Services, Conference Proceedings, pages 1–13, 2018.

[74] Chih-Chung Chang and Chih-Jen Lin. Libsvm: A library for support vector machines. *ACM Trans. Intell. Syst. Technol.*, 2(3):27:1–27:27, May 2011.

[75] Marc Saltzman. The latest in tiny technology: smart rings let you hide the phone but see alerts, discreetly, 2019. Retrieved December 7, 2019 from `https://www.usatoday.com/story/tech/columnist/saltzman/2018/05/15/smart-rings-let-you-hide-phone-but-keep-alerts/608336002/`.

[76] Amazon. Echo Loop, 2019. Retrieved December 7, 2019 from `https://www.amazon.com/Echo-Loop/dp/B07JPK4XJ6`.

[77] Mingming Fan and Khai N. Truong. Soqr: Sonically quantifying the content level inside containers. In *Proceedings of the 2015 ACM International Joint Conference on Pervasive and Ubiquitous Computing*, UbiComp '15, pages 3–14, New York, NY, USA, 2015. ACM.

[78] Gierad Laput, Xiang 'Anthony' Chen, and Chris Harrison. Sweepsense: Ad hoc configuration sensing using reflected swept-frequency ultrasonics. In *Proceedings of the 21st International Conference on Intelligent User Interfaces*, IUI '16, pages 332–335, New York, NY, USA, 2016. ACM.

[79] Munehiko Sato, Shigeo Yoshida, Alex Olwal, Boxin Shi, Atsushi Hiyama, Tomohiro Tanikawa, Michitaka Hirose, and Ramesh Raskar. Spectrans:

Versatile material classification for interaction with textureless, specular and transparent surfaces. In *Proceedings of the 33rd Annual ACM Conference on Human Factors in Computing Systems*, CHI '15, pages 2191–2200, New York, NY, USA, 2015. ACM.

[80] Hui-Shyong Yeo, Juyoung Lee, Andrea Bianchi, David Harris-Birtill, and Aaron Quigley. Specam: Sensing surface color and material with the front-facing camera of a mobile device. In *Proceedings of the 19th International Conference on Human-Computer Interaction with Mobile Devices and Services*, MobileHCI '17, pages 25:1–25:9, New York, NY, USA, 2017. ACM.

[81] Lennart Ljung. *System Identification: Theory for the User*. Prentice Hall, Upper Saddle River, NJ, USA, second edition, 1999.

[82] Nils Landin, Joseph M. Romano, William McMahan, and Katherine J. Kuchenbecker. Dimensional reduction of high-frequency accelerations for haptic rendering. In *Lecture Notes in Computer Science (including subseries Lecture Notes in Artificial Intelligence and Lecture Notes in Bioinformatics)*, volume 6192 LNCS, pages 79–86. Springer, Berlin, Heidelberg, 2010.

[83] Kenneth A Mann, Frederick W Wernere, and Andrew K Palmer. Frequency spectrum analysis of wrist motion for activities of daily living. *Journal of Orthopaedic research*, 7(2):304–306, 1989.

[84] M.A. Turk and A.P. Pentland. Face recognition using eigenfaces. In *Proceedings of the 1991 IEEE Computer Society Conference on Computer Vision*

and Pattern Recognition, CVPR '91, pages 586–591. IEEE Comput. Sco. Press, 1991.

[85] Won-Hyeong Park, Tae-Heon Yang, Yongjae Yoo, Seungmoon Choi, and Sang-Youn Kim. Flexible and bendable vibrotactile actuator using electro-conductive polyurethane. In *Proceedings of the IEEE World Haptics*, WHC '15, pages 165–170. IEEE, 2015.

[86] Won-Hyeong Park, Eun-Jae Shin, Sungryul Yun, and Sang-Youn Kim. An enhanced soft vibrotactile actuator based on epvc gel with silicon dioxide nanoparticles. *IEEE Transactions on Haptics*, 11(1):22–29, 2018.

[87] EPS News. mcube intros tiny mems accelerometer, November 2015.

[88] Gene F. Franklin, J. David Powell, and Michael L. Workman. *Digital Control of Dynamics Systems*. Addison-Wesley Publishing Company, Reading, MA, U.S.A., second edition, 1990.

[89] Karen E. MacLean. Foundations of transparency in tactile information design. *IEEE Transactions on Haptics*, 1(2):84–95, 2008.

[90] Seungmoon Choi and Katherine J. Kuchenbecker. Vibrotactile display: Perception, technology, and applications. *Proceedings of the IEEE*, 101(9):2093–2104, 2013.

[91] Oliver Schneider, Karon MacLean, Colin Swindell, and Kellogg Booth. Haptic experience design: What hapticians do and where they need help. *International Journal of Human-Computer Studies*, 107:5–21, 2017.

[92] Lung-Pan Cheng, Eyal Ofek, Christian Holz, Hrvoje Benko, and Andrew D. Wilson. Sparse haptic proxy: Touch feedback in virtual environments using a general passive prop. In *Proceedings of the 2017 CHI Conference on Human Factors in Computing Systems*, CHI '17, pages 3718–3728, New York, NY, USA, 2017. ACM.

[93] Yiwei Zhao, Lawrence H. Kim, Ye Wang, Mathieu Le Goc, and Sean Follmer. Robotic assembly of haptic proxy objects for tangible interaction and virtual reality. In *Proceedings of the 2017 ACM International Conference on Interactive Surfaces and Spaces*, ISS '17, pages 82–91, New York, NY, USA, 2017. ACM.

[94] Ben Lafreniere and Tovi Grossman. Blocks-to-CAD : A Cross-Application Bridge from Minecraft to 3D Modeling. In *Proceedings of the 31th Annual ACM Symposium on User Interface Software and Technology*, UIST '18, New York, NY, USA, 2018. ACM.

[95] Xiang 'Anthony' Chen, Stelian Coros, and Scott E. Hudson. Medley: A library of embeddables to explore rich material properties for 3d printed objects. In *Proceedings of the 2018 CHI Conference on Human Factors in Computing Systems*, CHI '18, pages 162:1–162:12, New York, NY, USA, 2018. ACM.

[96] Jonas Zehnder, Espen Knoop, Moritz Bächer, and Bernhard Thomaszewski. Metasilicone: Design and fabrication of composite silicone with desired

mechanical properties. *ACM Trans. Graph.*, 36(6):240:1–240:13, November 2017.

[97] Michal Piovarči, David I. W. Levin, Jason Rebello, Desai Chen, Roman Ďurikovič, Hanspeter Pfister, Wojciech Matusik, and Piotr Didyk. An interaction-aware, perceptual model for non-linear elastic objects. *ACM Trans. Graph.*, 35(4):55:1–55:13, July 2016.

[98] Ronald T. Verrillo. Temporal Summation in Vibrotactile Sensitivity. *The Journal of the Acoustical Society of America*, 37(5):843–846, may 1965.

[99] Alan K. Goble, Amy A. Collins, and Roger W. Cholewiak. Vibrotactile threshold in young and old observers: The effects of spatial summation and the presence of a rigid surround. *The Journal of the Acoustical Society of America*, 99(4):2256–2269, 1996.

[100] P J Lamoré and C J Keemink. Evidence for different types of mechanoreceptors from measurements of the psychophysical threshold for vibrations under different stimulation conditions. *The Journal of the Acoustical Society of America*, 83(6):2339–51, 1988.

[101] Miyuki Morioka and Michael J. Griffin. Thresholds for the perception of hand-transmitted vibration: Dependence on contact area and contact location. *Somatosensory and Motor Research*, 22(4):281–297, 2005.

[102] Ali Israr, Seungmoon Choi, and Hong Z. Tan. Detection threshold and mechanical impedance of the hand in a pen-hold posture. In *IEEE In-*

ternational Conference on Intelligent Robots and Systems, pages 472–477. IEEE, oct 2006.

[103] Ali Israr, Seungmoon Choi, and Hong Z. Tan. Mechanical Impedance of the Hand Holding a Spherical Tool at Threshold and Suprathreshold Stimulation Levels. In *Second Joint EuroHaptics Conference and Symposium on Haptic Interfaces for Virtual Environment and Teleoperator Systems (WHC'07)*, pages 56–60. IEEE, mar 2007.

[104] Miyuki Morioka and Michael J. Griffin. Absolute thresholds for the perception of fore-and-aft, lateral, and vertical vibration at the hand, the seat, and the foot. *Journal of Sound and Vibration*, 314(1-2):357–370, jul 2008.

[105] Jonghyun Ryu, Jaehoon Jung, Gunhyuk Park, and Seungmoon Choi. Psychophysical model for vibrotactile rendering in mobile devices. *Presence: Teleoperators and Virtual Environments*, 19(4):364–387, aug 2010.

[106] N Harada and M J Griffin. Factors influencing vibration sense thresholds used to assess occupational exposures to hand transmitted vibration. *Occupational and Environmental Medicine*, 48(3):185–192, mar 1991.

[107] Angela DiDomenico and Maury A. Nussbaum. Estimation of forces exerted by the fingers using standardised surface electromyography from the forearm. *Ergonomics*, 51(6):858–871, jun 2008.

[108] R W Cholewiak, C E Sherrick, and A A Collins. Princeton Cutaneous Research Project (Report# 60). *Unpublished manuscript, Princeton University, Department of Psychology*, 1992.

[109] H. Levitt. Transformed Up-Down Methods in Psychoacoustics. *The Journal of the Acoustical Society of America*, 49(2B):467–477, feb 1971.

[110] tangerineX. Tutorial 1: How to specify vibration intensity in sensation level. `http://www.tangerinex.com/sensation_level.html`. Last accessed on April 16, 2019.

[111] Kenneth O. Johnson. The roles and functions of cutaneous mechanoreceptors. *Current Opinion in Neurobiology*, 11(4):455–461, 2001.

[112] S. Aatola. Transmission of vibration to the wrist and comparison of frequency response function estimators. *Journal of Sound and Vibration*, 131(3):497–507, 1989.

[113] Ronald T. Verrillo. Effect of Contactor Area on the Vibrotactile Threshold. *The Journal of the Acoustical Society of America*, 35(12):1962–1966, 1963.

[114] Ronald T. Verrillo. Vibrotactile thresholds measured at the finger. *Perception & Psychophysics*, 9(4):329–330, jul 1971.

Acknowledgements

Human-Computer Interaction이라는 학문 분야에 대해서 처음 알게 되었을 때, 진심으로 도전해보고 싶다는 마음이 들었습니다. 대학원 학위 과정 동안 많은 어려움과 힘든 시기들이 있었지만 많은 분의 가르침과 도움을 받아서 학위 과정을 성공적으로 마무리 할 수 있었습니다. 제 막연한 관심과 흥미가 구체화 되어 결실을 볼 수 있도록 지도해주신 최승문 교수님께 깊은 감사의 인사를 드립니다. 교수님께 학문적으로 또 인간적으로 가르침을 받을 수 있었던 것은 정말 큰 행운이었습니다. 앞으로도 교수님의 가르침을 마음에 새기고 그 가르침이 세상을 널리 이롭게 하도록 하겠습니다. 연구에 첫발을 함께 내디뎌 주신 소효정 교수님, 어려운 처지의 저를 거둬주셨던 정민근 교수님, 학부 지도 교수님이신 정윤하 교수님, 헤매고 있었던 저에게 약이 되는 깨우침을 주신 강봉구 교수님께도 감사 인사를 드립니다.

HVR 연구실 생활을 함께하면서 선배로서 많은 도움을 주었던 종만이 형, 건혁이 형, 레자 형, 아미트 형, 호진이 형, 용재 형, 그리고 성환이에게 감사하다는 말을 전하고 싶습니다. 제 연구에 관심을 가지고 지칠 때마다 힘을 실어줬던 건혁이 형 감사합니다. 함께 많은 추억을 만들고 고생한 후배들인 호준이, 인석이, 성호, 한슬이, 상윤이, 종호, 겨레, 선웅, 성원이, 혜진이, 효승이, 채용이, 지완이, 범수, 기홍이, 준경이, 진수에게도 앞으로의 길을 항상 응원한다고 전하고 싶습니다. 특히, 까다로운 선배랑 같이 연구하느라고 고생한 겨레, 진수, 그리고 채용이에게는 미안하다는 말도 꼭 하고 싶습니다. 그리고 새벽반으로 힘들 때마다 같이 이야기를 많이 나눠준 호진이 형과 호준이에게도 이제는 생체 시계를 돌리자는 말을 남깁니다. HDT 연구실에서 함께 동고동락했던 규동이 형과 순모, 첫 사수로써 저에게 많은 도움을

주었던 희진 누나, 공학 4동에서 가장 오랫동안 함께한 동영이, HSD 연구실에서 저를 따듯하게 맞이해주었던 충식이 형, 보라 누나, 그리고 민규, 함께 운동하고 서로 응원해줬던 대학원 동기들인 기영이 형, 병화, 영빈이, 그리고 희승이에게도 감사하다는 말을 남기고 싶습니다.

마지막으로 12년이라는 시간을 포항에서 보내는 동안 가장 큰 힘이 되어주셨던 부모님과 외할머니께 감사드립니다. 언제나 묵묵히 응원해주신 아버지, 항상 제 마음을 헤아려주신 어머니, 그리고 저를 항상 걱정해주시는 외할머니가 든든하게 계셔서 학위 과정을 잘 마칠 수 있었던 것 같습니다. 남들보다는 조금 긴 25년이라는 시간을 학생으로 공부를 하고 세상에 나가면서 한편으로 조금은 두렵기도 하지만 언제나 어디서나 초심을 잃지 않고 정진하도록 하겠습니다.

Publications

International Journal

1. **Seungjae Oh**, Jinhyuk Yoon, Chaeyong Park, and Seungmoon Choi. Identification of contact finger(s) on rigid surfaces with Vibration Ring and Microphone. In Preparation.

2. **Seungjae Oh** and Seungmoon Choi. Effects of Contact Force and Vibration Frequency on Vibrotactile Sensitivity During Active Touch. *IEEE Transactions on Haptics*, 12 (4), pp. 645-651, 2019.

3. Heejin Kim, **Seungjae Oh**, Sung H. Han, and Min K. Chung. Motion–Display Gain: A New Control–Display Mapping Reflecting Natural Human Pointing Gesture to Enhance Interaction with Large Displays at a Distance. *International Journal of Human–Computer Interaction*, 35 (2), pp. 180-195, 2019.

4. **Seungjae Oh**, Hyo-Jeong So, and Matthew Gaydos. Hybrid Augmented Reality for Participatory Learning: The Hidden Efficacy of Multi-User Game-Based Simulation. *IEEE Transactions on Learning Technologies*, 11 (1), pp. 115-127, 2018.

International Conference: Paper

1. Jinsoo Kim*, **Seungjae Oh***, Chaeyong Park, and Seungmoon Choi (*Co-first Author). Body-Penetrating Tactile Phantom Sensations. In *Proceedings of the 2020 CHI conference on Human Factors in Computing Systems* (CHI '20), Accepted for Publication, 2020.

2. **Seungjae Oh**, Gyeore Yun, Chaeyong Park, Jinsoo Kim, and Seungmoon Choi. VibEye: Vibration-Mediated Object Recognition for Tangible Interactive Applications. In *Proceedings of the 2019 CHI conference on Human Factors in Computing Systems* (CHI '19), Paper 676, 2019.

3. Gyeore Yun, **Seungjae Oh**, and Seungmoon Choi. Seamless Phantom Sensation Moving across a Wide Range of Body. In *Proceedings of the 2019 IEEE World Haptics Conference* (WHC '19), pp. 616-621, 2019.

4. Chaeyong Park, Jaeyoung Park, **Seungjae Oh**, and Seungmoon Choi. Realistic Haptic Rendering of Collision Effects Using Multimodal Vibrotactile and Impact Feedback. In *Proceedings of the 2019 IEEE World Haptics Conference* (WHC '19), pp. 449-454, 2019.

5. Sei-Young Kim, Hyo-Jeong So, Soonmo Kwon, **Seungjae Oh**, Kyudong Park, Minjin Ko, Jaewon Yoo, and Gyuhwan Oh. Towards Designing a Mobile Social Learning Application with Meaningful Gamification Strategies. In *Proceedings of the 2015 IEEE International Conference on Advanced Learning Technologies* (ICALT '15), pp. 170-174, 2015.

6. Kyudong Park, **Seungjae Oh**, Heung-Chang Lee, and Hyo-Jeong So. Dynamic Feedback Mechanism for Maximizing Interaction in Online Social Network Services. In *Proceedings of the 2014 IEEE/ACM Conference on Advances in Social Networks Analysis and Mining* (ASONAM '14), pp. 844-849, 2014.

International Conference: Poster and Demonstration

1. **Seungjae Oh**, Gyeore Yun, Chaeyong Park, Jinsoo Kim, and Seungmoon Choi. VibEye: A System for Identification of Hand-held Object by Visualizing Vibration Propagation Dynamics. In *Proceedings of the 2019 IEEE World Haptics Conference* (WHC'19), 2019.

2. Chaeyong Park, Jaeyoung Park, **Seungjae Oh**, and Seungmoon Choi. Realistic Haptic Rendering of Collision Effects Using Multimodal Vibrotactile and Impact Feedback. In *Proceedings of the 2019 IEEE World Haptics Conference* (WHC'19), 2019.

3. Gyeore Yun, **Seungjae Oh**, and Seungmoon Choi. Seamless Phantom Sensation Moving Across a Wide Range of Body. In *Proceedings of the 2019 IEEE World Haptics Conference* (WHC'19), 2019.

4. **Seungjae Oh**, Kyudong Park, Soonmo Kwon, and Hyo-Jeong So. Designing a Multi-user Interactive Simulation Using AR Glasses. In *Proceedings of the 10th International Conference on Tangible, Embedded, and Embodied Interaction* (TEI '16), pp. 539-544, 2016.

5. Soonmo Kwon, **Seungjae Oh**, Kyudong Park, Sei-young Kim, and Hyo-Jeong So. Children s Participatory Designers of a New Type of Mobile Social Learning Application. In *Proceedings of the 17th International Conference on Human-Computer Interaction with Mobile Devices and Services Adjunct* (Mobile HCI '15), pp. 862-869, 2015.

6. Heejin Kim, **Seungjae Oh**, Sung H Han, and Min K Chung. Natural Pointing Posture in Distal Pointing tasks. In *Proceedings of the 2nd ACM symposium on Spatial user interaction* (SUI '14), pp. 148-148, 2014.

7. **Seungjae Oh**, Heejin Kim, and Hyo-Jeong So. Proposing a Classification Model for Perceptual Target Selection on Large Displays. In *Proceedings of the 2nd ACM symposium on Spatial user interaction* (SUI '14), pp. 151-151, 2014.

8. **Seungjae Oh**, Hee-Seung Kwon, and Hyo-Jeong So. Hidden UI: Projection-based Augmented Reality for Map Navigation on Multi-touch Tabletop. In *Proceedings of the 2nd ACM symposium on Spatial user interaction* (SUI '14), pp. 162-162, 2014.

9. **Seungjae Oh**, Heejin Kim, and Min K Chung. Understanding of Spatial Gestural Motor Space: a Study on Cursorless Absolute Freehand Pointing on Large Displays. In *Proceedings of the 2014 IEEE Symposium on 3D User Interfaces* (3DUI '14), pp. 167-168, 2014.

Curriculum Vitae

Name : Seungjae Oh

Education

2008 – 2012	Department of Electrical Engineering, Pohang University of Science and Technology (B.S.)
2012 – 2020	Department of Creative IT Engineering, Pohang University of Science and Technology (Ph.D.)

Affiliation

1. Haptic and Virtual Reality Lab., Department of Computer Science and Engineering, Pohang University of Science and Technology
2. Human-centered Design and Technology Lab., Department of Creative IT Engineering, Pohang University of Science and Technology
3. Human System Design Lab., Department of Industrial Engineering, Pohang University of Science and Technology